

# Water Resources Research

## RESEARCH ARTICLE

10.1029/2018WR024289

### Key Points:

- A numerical experiment was used to improve understanding of uncertainty propagation in coupled hydrologic-hydraulic models
- Discrepancies in measured and simulated flow peaks lead to large uncertainties in predicted floodplain inundation volumes and extent
- The challenges of multiyear continuous modeling are highlighted with an event-based approach recommended

### Supporting Information:

- Supporting Information S1

### Correspondence to:

S. Grimaldi,  
Stefania.Grimaldi@monash.edu

### Citation:

Grimaldi, S., Schumann, G. J.-P., Shokri, A., Walker, J. P., & Pauwels, V. R. N. (2019). Challenges, opportunities and pitfalls for global coupled hydrologic-hydraulic modeling of floods. *Water Resources Research*, 55. <https://doi.org/10.1029/2018WR024289>

Received 20 OCT 2018

Accepted 20 MAY 2019

Accepted article online 3 JUN 2019

## Challenges, Opportunities, and Pitfalls for Global Coupled Hydrologic-Hydraulic Modeling of Floods

S. Grimaldi<sup>1</sup> , G. J.-P. Schumann<sup>2,3</sup> , A. Shokri<sup>1</sup> , J. P. Walker<sup>1</sup> , and V. R. N. Pauwels<sup>1</sup> 

<sup>1</sup>Department of Civil Engineering, Monash University, Clayton, Victoria, Australia, <sup>2</sup>School of Geographical Sciences, University of Bristol, Bristol, UK, <sup>3</sup>Remote Sensing Solutions Inc., Barnstable, MA, USA

**Abstract** Flood modeling at the regional to global scale is a key requirement for equitable emergency and land management. Coupled hydrological-hydraulic models are at the core of flood forecasting and risk assessment models. Nevertheless, each model is subject to uncertainties from different sources (e.g., model structure, parameters, and inputs). Understanding how uncertainties propagate through the modeling cascade is essential to invest in data collection, increase flood modeling accuracy, and comprehensively communicate modeling results to end users. This study used a numerical experiment to quantify the propagation of errors when coupling hydrological and hydraulic models for multiyear flood event modeling in a large basin, with large morphological and hydrological variability. A coupled modeling chain consisting of the hydrological model Hydrologiska Byråns Vattenbalansavdelning and the hydraulic model LISFLOOD-FP was used for the prediction of floodplain inundation in the Murray Darling Basin (Australia), from 2006 to 2012. The impacts of discrepancies between simulated and measured flow hydrographs on the predicted inundation patterns were analyzed by moving from small upstream catchments to large lowland catchments. The numerical experiment was able to identify areas requiring tailored modeling solutions or data collection. Moreover, this study highlighted the high sensitivity of inundation volume and extent prediction to uncertainties in flood peak values and explored challenges in time-continuous modeling. Accurate flood peak predictions, knowledge of critical morphological features, and an event-based modeling approach were outlined as pragmatic solutions for more accurate prediction of large-scale spatiotemporal patterns of flood dynamics, particularly in the presence of low-accuracy elevation data.

**Plain Language Summary** Floods are among the most devastating natural hazards, affecting multiple regions and millions of people each year. Accurate inundation predictions are vital information for land and emergency management. This objective can be achieved through a cascade of numerical models. However, each model is subject to uncertainties from different sources (e.g., input data, model structure, and parameters), and an understanding of how these uncertainties are propagated through each step of the modeling cascade is pivotal to improving inundation prediction accuracy. This study investigated the impact of uncertainties in streamflow predictions on the accuracy of floodplain inundation predictions. For this purpose, the Murray Darling Basin (Australia), a large basin that is affected by destructive floods, was used as a case study. The analysis illustrated the high sensitivity of floodplain inundation predictions to predicted streamflow peak values. Moreover, when attempting to model a long time series of low- and high-flow periods, uncertainties in the inundation patterns increased over time and from upstream to downstream areas of the basin. These results demonstrated the need for accurate predictions of streamflow peak values and suggested that focusing on the modeling of each large flood event separately is a more effective strategy for reliable inundation predictions.

### 1. Introduction

Floods are among the most devastating natural hazards, affecting multiple regions and millions of people each year. According to the United Nations, from 1995 through 2015, flooding alone accounted for 47% of all weather-related disasters worldwide, affecting 2.3 billion people (Wahlstrom & Guha-Sapir, 2015). Accurate flood modeling is one indispensable tool for improving predictions, increasing resilience, and reducing economic losses of such events. A modeling cascade composed of a numerical weather prediction model for the estimation of precipitation and meteorological variables, a hydrological model for the simulation of rainfall-runoff processes and the assessment of streamflow rates, and a hydraulic model for streamflow routing and estimating floodplain inundation dynamics should be at the core of any flood forecasting system and flood risk assessment model.

Cascading from rainfall to floodplain dynamics is thus a pivotal component of any flood forecast and flood risk analysis, and a number of studies have focused on the coupling of hydrologic and hydraulic models, particularly at the catchment scale. In a pioneering study, Pappenberger et al. (2005) developed a coupled flood model for the Meuse catchment (Belgium). Lian et al. (2007) then demonstrated that the use of the coupled modeling approach could adequately predict peak flow time in the Illinois River Basin (USA); Kleynhans et al. (2007) used this concept to analyze the impact of planning scenarios on the ecology of the Nyl River in South Africa; and Bonnifait et al. (2009) studied a single catastrophic flood event in France. The coupling approach was used by Gül et al. (2010) to test the efficiency of structural flood control measures and by Mejia and Reed (2011) to investigate the effects of parameterized cross section shapes on inundation modeling. This model combination was also applied in an urban context by Domingo et al. (2010), Nania et al. (2014), and Zhu et al. (2016). A few studies focused on the merging of remote sensing data with coupled models. Montanari et al. (2009) calibrated a hydraulic model using remotely sensed flood extents, and used this information to update the hydrologically modeled soil moisture values. Matgen et al. (2010) sequentially updated the modeled water levels of a coupled model in a synthetic study, while Giustarini et al. (2011) performed this updating using real (as opposed to synthetic) data. Instead of using observed rainfall records as model input, Nam et al. (2014) used results from a numerical weather prediction model as input to the sequence of models for short-term flood inundation prediction. Laganier et al. (2014), Nguyen et al. (2016), and Mai and De Smedt (2017) showed that the coupled approach can adequately model flash floods and floodplain inundation. A coupled hydrologic-hydraulic modeling approach was recommended by Grimaldi et al. (2013) for flood hazard modeling, by Felder et al. (2017) for probable maximum flood risk estimation, and by Sindhu and Durga (2017) for flood damage mitigation. The potential of a coupled modeling approach to identify and predict flood prone areas in ungauged catchments was recently shown by Komi et al. (2017) using the Oti River Basin (West Africa) as case study.

Albeit flood risk assessment and real-time forecasting have been traditionally undertaken at catchment and national scales, recent improvements in global data sets, numerical algorithms, computing power, and coupled modeling frameworks have allowed the development and execution of flood models at the continental and global scales (e.g., Alfieri et al., 2013; Wu et al., 2014). These large-scale flood models allow consistent and equitable decision making (Thielen-del Pozo et al., 2015; Ward et al., 2015), and their application in developing countries and data-scarce regions can be extremely helpful to reduce catastrophic impacts, as demonstrated by the activities of the Global Flood Partnership (Alfieri et al., 2018).

Operational global- and continental-scale flood forecasting systems are currently based on a weather prediction module and a rainfall-runoff hydrological module (Emerton et al., 2016). However, inclusion of two-dimensional hydraulic models into large-scale flood forecast and risk assessment systems has been advocated by a number of studies (e.g., Falter et al., 2016; Falter et al., 2015; Huang & Hattermann, 2018; Schumann et al., 2016; Vorogushyn et al., 2018; Zhao et al., 2017) because it enables more accurate predictions of floodplain inundation dynamics. Moreover, Bates et al. (2018) highlighted the need to use hydraulic models to predict the duration of flooding, as this parameter largely affected the impacts of flood events in a number of recent disasters, such as the floods in Queensland (Australia) in 2010–2011, in Thailand in 2011, in England and Wales (UK) in 2014, and, more recently, the 2017 hurricane floods in the United States. Nevertheless, the technical hurdles (mainly, data availability and computational power) that have so far hindered routine implementation of two-dimensional hydraulic models at the large scale are sensibly diminishing (e.g., Bates et al., 2018; Moretti & Orlandini, 2017; Neal et al., 2018), and recently, large-scale flood modeling approaches have begun to couple hydrologic and hydraulic models. For instance, Biancamaria et al. (2009) optimized the river depth and roughness coefficient of a coupled system for the Ob River in Western Siberia; Yamazaki et al. (2013) applied a new river routing model to provide global flood hazard maps, and the same model was used by Hirabayashi et al. (2013) to produce global flood risk maps under climate change. Schumann et al. (2013) then used remote sensing data to calibrate and evaluate a coupled hydrologic-hydraulic model of the Zambezi River (Mozambique), Alfieri et al. (2014) derived a flood hazard map for Europe using a long-term streamflow simulation, Sampson et al. (2015) produced global flood hazard maps at 3-arc-sec resolution for several return periods, and Dottori et al. (2016) proposed an evaluation framework for global flood hazard mapping. More recently, Dottori et al. (2018) coupled hydrological models with the mass-conservative routing scheme presented in Yamazaki et al. (2011) to estimate

human losses and economic impacts of river flooding at the global scale under a range of climate change scenarios.

However, each component of the flood modeling chain is subject to uncertainties from different sources (e.g., model structure, parameters, and inputs). Improving the understanding of the propagation of these uncertainties through the modeling cascade is essential to pinpoint strategies to define areas of further investigation, invest in data collection, improve model accuracy, and comprehensively communicate modeling results to end users (e.g., Trigg et al., 2016; Ward et al., 2015). Such a rigorous assessment requires identification of all the sources of uncertainty within the modeling cascade and results in a large number of model runs with extremely high computational costs, especially when using distributed models (e.g., Pappenberger et al., 2005). Simplified approaches designed to reduce the computational burden of uncertainty estimation were applied, for instance, by Pappenberger et al. (2005), McMillan and Brasington (2008), and Rodríguez-Rincón et al. (2015) for event-based analysis; by Falter et al. (2016) in a continuous modeling approach; and by Sampson et al. (2014) and Zischg et al. (2018) in a flood damage assessment model.

More specifically, Pappenberger et al. (2005) applied a simplified generalized likelihood uncertainty estimation (GLUE) approach to predict the 1995 flood in the Meuse River (Belgium). In this case study, uncertainties in the ensemble rainfall-runoff predictions had limited impact on the floodplain inundation extent uncertainty. However, inundation-level uncertainties due to erroneous discharge predictions increased from upstream to downstream (i.e., moving away from the input point), especially in regions of constricted flow. McMillan and Brasington (2008) similarly applied a simplified GLUE methodology for the definition of probabilistic maps of flood extent with 10- to 1,000-year return period in the Granta River (UK). They showed that inundation extents were more sensitive to uncertainty in rainfall-runoff modeling than to variations in the main hydraulic model parameter (i.e., hydraulic roughness). Rodríguez-Rincón et al. (2015) used a hindcast scenario to study the propagation of meteorological and hydrological model uncertainties to the results of a hydraulic model used for the prediction of inundation extents in the 2009 flood of the Tonalá River (Mexico). The case study was a valley filling event, and all hydraulic simulations produced similar inundation extents, with small propagation of meteorological and hydrological errors to the flood map. Falter et al. (2016) presented a modeling cascade for continuous, large-scale flood risk assessments. The approach was applied to the Elbe catchment (Germany) for the period of 1990–2003, and uncertainties were evaluated, where possible, with observed data. Here low-quality topographic data and lack of representation of dike breaches caused large uncertainties in the results of the hydraulic model. Sampson et al. (2014) and Zischg et al. (2018) analyzed the impact of uncertain precipitation data on loss estimates in Dublin (Ireland) and in the Aare River basin (Switzerland), respectively. Loss estimates had high sensitivity to relatively small percentage changes in hydrograph peak or volume and, as previously shown by Neal et al. (2013), to superimposition of the flood peaks between tributaries.

The above studies identified large variability of the impact of discharge hydrographs inaccuracy and uncertainty on floodplain inundation extent as a function of catchment morphology and flood event characteristics. A better understanding of the impact of uncertainties of simulated flow hydrographs on the output of hydraulic models is therefore required (Dottori et al., 2016; Schumann et al., 2013) to meet the need for more accurate flood modeling for both current risk and climate change projections (e.g., Bates et al., 2018; Trigg et al., 2016). Consequently, to add to the current state of knowledge in large-scale flood modeling and prediction, this study aims to investigate the propagation of errors when coupling hydrological and hydraulic models. For this purpose, a numerical experiment was designed to develop a novel quantitative analysis of the impact of discrepancies between simulated and measured time series of discharge data on the prediction of long-term patterns of floodplain inundation volumes and extents in a large basin, where morphological and hydrological features vary spatially. A quantitative methodology for the comparison of input discrepancies and discrepancies in floodplain inundation dynamics was introduced to (1) investigate whether discrepancies in input time series are enhanced or damped by the hydraulic model for the prediction of floodplain inundation volumes and extents; (2) identify causes for such effects; (3) investigate whether continuous, long-term modeling of low and high flow diminishes or exacerbates the problem; and (4) clarify how input-driven discrepancies in floodplain inundation predictions propagate from upstream to downstream. The methodology was applied to a state-of-the-art modeling framework that was implemented in a large basin with large morphological and hydrological variability. More specifically, the coupled modeling chain consisted of two widely used models, that is, the hydrological model

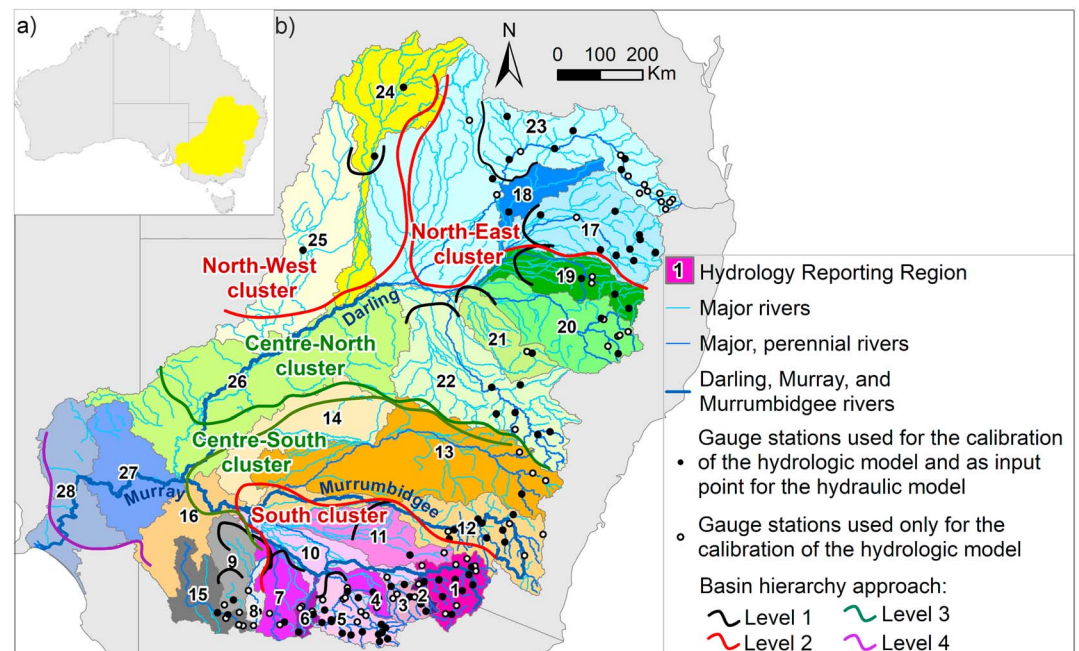


**Figure 1.** Study area. (a) Location of the Murray Darling Basin. (b) Murray Darling Basin: river network; discharge gauge stations; 28 Hydrology Reporting Regions; areal subdivision according to the basin hierarchy approach (section 3.3.1).

Hydrologiska Byråns Vattenbalansavdelning (HBV; Lindström et al., 1997) and the hydraulic model LISFLOOD-FP (Bates et al., 2010; Neal, Schumann, & Bates, 2012). Simulated and measured discharge time series were alternatively used as input to LISFLOOD-FP for the prediction of floodplain inundation volumes and extents in the Murray Darling Basin (MDB; Australia) from 2006 to 2012. According to this experimental design, differences between simulated and measured discharge time series were known, and this knowledge allowed quantifying the impacts of discrepancies in forcing data on the prediction of inundation volumes and extent. Moreover, the cascading of discrepancies in floodplain inundation predictions during consecutive low- and high-flow periods and their interactions at different spatial scales, from small upstream catchments to larger lowland catchments, were analyzed according to hydrograph characteristics (e.g., total input volume and flood peak values).

The numerical experiment presented here identified the main drivers exacerbating the impacts of differences in forcing data on the prediction of inundation volumes and extents. Based on the results of this study, recommendations for more accurate predictions of the spatiotemporal patterns of surface water extent and flood dynamics at the large (basin, continental, or global) scale were formulated.

## 2. Study Area and Data

The study area used here is the MDB, located in the southeast of Australia (Figure 1a). The MDB is a large semiarid region that covers  $1 \times 10^6$  km<sup>2</sup>, being 14% of Australia's land area and containing Australia's three longest rivers, the Darling (2,740 km), Murray (2,530 km), and Murrumbidgee (1,690 km). The MDB generates 39% of the national income derived from agricultural production, it includes over 30,000 wetlands, and it is home to a number of endangered species of birds, fish, and mammals (Murray-Darling Basin Authority, 2010; <https://www.murraydarlingwetlands.com.au/wetlands/quick-facts.asp>).

The MDB is subject to El Niño-Southern Oscillation-induced climatic variability with long dry spells, punctuated by large flood events (Arthington & Balcombe, 2011; Bunn et al., 2006). This variability was recently exacerbated by the Millennium Drought from the mid-1990s to 2009, which was followed by extreme floods in 2010–2011, commonly referred to as the La Niña floods (Leblanc et al., 2012). The MDB has a pronounced climate gradient with average annual rainfall decreasing and climate variability and evapotranspiration increasing from the southeast to the northwest (Murray-Darling Basin Authority, 2010). Due to this climate gradient, flooding regimes differ substantially across the MDB, with many of the ephemeral catchments in

the northern area affected by intensive flood bursts in the summer months and rivers in the southern area typically affected by long flood events driven by rainfall and snowmelt in winter and spring (Bunn et al., 2006; Penton & Overton, 2007).

The river network is composed of 119 major rivers, of which 71 are perennial (Figure 1b). The Australian Hydrological Geospatial Fabric (Australian Bureau of Meteorology, 2015) delineates the boundaries of 28 drainage divisions (Hydrology Reporting Regions [HRR]). Drainage divisions are the key data set for hydrological analysis (e.g., Huang et al., 2013); in this study drainage divisions were allocated to the North-East, North-West, Centre-North, South, and Centre-South areas of the basin as seen in Figure 1b and as further explained in section 3.3.1.

### 3. Methods

#### 3.1. Hydrologic Model

The hydrologic model used in this study was the HBV model (Lindström et al., 1997). The HBV is a lumped conceptual model that uses precipitation and potential evapotranspiration as input. For streamflow prediction, the precipitation is partitioned into a soil reservoir, a slow reservoir, and a fast reservoir. Modeled streamflow is then routed to the catchment outlet using a triangular unit hydrograph. The three reservoirs and the unit hydrograph are characterized by nine parameters. A detailed description of the HBV model can be found in Pauwels et al. (2013).

Model simulations were performed for a 7-year period, from 1 January 2006 through 31 December 2012, at a daily time step. Measured daily precipitation data in the form of  $0.01^\circ$  maps are provided by the Australian Bureau of Meteorology and stored in the Australian National University Climate database. Monthly  $0.01^\circ$  maps of potential evapotranspiration data were generated by the eMAST-R Package (Xu et al., 2018). Both data sets are available from the Australian National Computational Infrastructure (Jones et al., 2009). Hourly time series of discharge observations at 148 gauge stations (Figure 1b, full and hollow black dots) were available from the following agencies and government services: New South Wales Office of Water, Queensland Department of Natural Resources and Mines, and Victoria Department of Environment and Primary Industries.

The model was calibrated using particle swarm optimization (Kennedy & Eberhart, 1995) in order to minimize the root mean square deviation (*RMSD*, equation 10, Table 1) between simulated and measured discharge values, denoted by *h<sub>bv</sub>* and *g*, respectively (Table 1). A specific calibration for high flows is currently not routinely included in the forecast framework at large and global scales (Hirpa et al., 2018) and was not implemented here. The performance of the calibrated model was evaluated by computing the Nash-Sutcliffe (*NS*) efficiency (Nash & Sutcliffe, 1970; equation 12, Table 1) over the 148 modeled subcatchments of the MDB. The highest and lowest *NS* values were 0.92 and 0.04, respectively; the quartiles were 0.24, 0.42, 0.59, and 0.75. These results indicated that the calibrated model can adequately simulate the rainfall-runoff processes in a basin with a large hydrological variability. This model performance was deemed adequate for the purpose of this study, which was not the accurate reproduction of real events but the analysis of the impacts of plausible discrepancies between simulated and measured flows on floodplain inundation dynamics within the current flood forecasting framework at the large scale.

#### 3.2. Hydraulic Model

LISFLOOD-FP, a computationally efficient two-dimensional hydraulic model (Bates et al., 2010), was used to generate large-scale flood inundation across the MDB. LISFLOOD-FP operates on a regular grid, with water flow through each model grid cell simulated by solving the inertial momentum equation through a single explicit finite difference scheme. This simplified form only neglects the convective acceleration term in the full shallow water equations and thereby overcomes limitations related to considerable time step decreases in explicit diffusive models that also neglect local inertia. The continuity equation is then used to update water depths at each time step. The resulting model is simple yet contains enough physics to describe flood processes adequately while requiring an order of magnitude fewer computational operations than does a full shallow water model (Neal, Villanueva, et al., 2012). Moreover, the model can simulate river and floodplain hydraulics at relatively coarse spatial resolutions by using a subgrid formulation that allows river channels with widths smaller than those of the nominal model resolution (Neal, Schumann, & Bates, 2012).

For this study, the setup of the subgrid formulation of LISFLOOD-FP was the same as in the continental-scale version presented in Schumann et al. (2016). Terrain morphology was represented by the freely available Shuttle Radar Topography Mission (SRTM) digital elevation model (DEM), which was corrected for vegetation canopy height using the global Ice, Cloud, and land Elevation Satellite (ICESat-1) canopy data set (Simard et al., 2011) as explained in Schumann et al. (2013). The Surface Network provided by the Australian Hydrological Geospatial Fabric (Australian Bureau of Meteorology, 2015) was used to identify river cells; channel bathymetry was then estimated within the model code using the methodology proposed by Neal, Schumann, and Bates (2012) and global parameters presented in Andreadis et al. (2013). Compared to the continental-scale version, the only difference was that all major rivers in the MDB, rather than just the rivers draining areas over 10,000 km<sup>2</sup>, were explicitly represented in this study (Figure 1b). The continental-scale model configuration was calibrated on the 1995 flood event in the Murrumbidgee River (HRR 12); inundation extents predicted by a 40-year model run were then compared to a multiyear remote sensing-derived maximum extent (Mueller et al., 2016), resulting in a correct predicted flooding statistic of 89.6% and an area in error of 10.9% (Schumann et al., 2016). Accurate regional calibration of hydraulic models is extremely time and data demanding (Dottori et al., 2016), and discrepancies in input data are expected to have larger impacts on the prediction of floodplain dynamics than do model parameters (e.g., McMillan & Brasington, 2008). Consequently, the use of the same model parameterization as the continental-scale version was considered a pragmatic, effective solution for the purpose of providing a realistic representation of inundation dynamics. The model implementation also included lakes and reservoirs from the Global Lake and Wetland Database (Lehner & Döll, 2004). Reservoirs and channels were filled with an average water level before starting the computations and were handled implicitly within the model numerical scheme, without any operational rules or sudden water releases. In other words, the model used the same numerical scheme everywhere, including across the surface of lakes and reservoirs. Moreover, agricultural, industrial, or other water withdrawals that were not already captured by a stream gauge were not accounted for in the current model setup. The simplifications and assumptions listed above clearly affect model results, and more research is needed to understand how to correctly implement highly nontrivial elements such as reservoir operations and water withdrawals in hydraulic models. However, albeit relatively simple, the model setup used in this study can be considered a best first effort for the representation of floodplain inundation dynamics in the MDB.

The model was forced using daily discharge time series at 81 input points; these input points were the gauge stations located along the major river network (Figure 1b, full black dots). Downstream boundary conditions were imposed using the thalweg gradient as a normal depth flow condition. Since seasonal evaporative water loss is significant in the MDB (Leblanc et al., 2012), interpolated and gridded multiyear averages of daily satellite-derived evapotranspiration fields provided by the Global Land Evaporation Amsterdam Model (Martens et al., 2017; Miralles et al., 2011) were included in LISFLOOD-FP. More specifically, these losses were included in the model following the implementation by Neal, Schumann, and Bates (2012). Floodplain flow paths and inundation extents and volumes were simulated at 1-km resolution.

### 3.3. Coupled Modeling Approach and Data Analysis

The coupling between HBV and LISFLOOD-FP was external (offline) and unidirectional; that is, the continuous output from HBV was used as continuous input into LISFLOOD-FP. The two models remained independent from each other, meaning that important hydraulic effects, such as backwater, did not impact the hydrologic model. Nevertheless, backwater effects were expected to be small within the design of this study where HBV was used to model only upstream catchments and normal depth conditions were used as boundary conditions for LISFLOOD-FP. Consequently, such a relatively simple coupling strategy might affect model results, but the impacts of dynamic model feedback were assumed negligible when compared to the other sources of nontrivial uncertainty (e.g., the resolution and accuracy of the topographic data). Moreover, the use of dynamic coupling for the modeling of floodplain inundation dynamics at the large scale would require extremely large computational resources that hamper both the feasibility and transferability of the methodology to other study areas (Laganier et al., 2014; Lerat, 2009). Conversely, external unidirectional coupling has been successfully applied in a number of previous analyses (Bravo et al., 2012; Lian et al., 2007; Mejia & Reed, 2011), and it was hence considered a sensible approach for the purposes of this study. In fact, more research is needed to effectively incorporate dynamic model feedback in a coupled

**Table 1**  
Symbols and Performance Metrics Used for the Continuous and Event-Based Time Series Analysis

Definitions		Symbols
<ul style="list-style-type: none"> <li>Cumulative input volume</li> </ul>		$hbv_i$ = monthly (daily) input volume predicted by HBV for month (day) $i$
Simulated by HBV: $iv, HBV(\alpha, \beta) = \sum_{i=\alpha}^{\beta} (hbv_i)$	(1)	
Measured: $iv, G(\alpha, \beta) = \sum_{i=\alpha}^{\beta} (g_i)$	(2)	$g_i$ = monthly (daily) input volume measured by the gauge stations for month (day) $i$
<ul style="list-style-type: none"> <li>Increment of floodplain inundation volume</li> </ul>		$fv, HBV_i$ = monthly maximum floodplain inundation volume predicted by LISFLOODFP-HBV for month $i$
LISFLOODFP-HBV: $fv, HBV(\alpha, \beta) = fv, HBV_{\beta} - fv, HBV_{\alpha}$	(3)	
LISFLOODFP-MEAS: $fv, G(\alpha, \beta) = fv, G_{\beta} - fv, G_{\alpha}$	(4)	
<ul style="list-style-type: none"> <li>Increment of floodplain inundation extent</li> </ul>		$fv, G_i$ = monthly maximum floodplain inundation volume predicted by LISFLOODFP-MEAS for month $i$
LISFLOODFP-HBV: $fe, HBV(\alpha, \beta) = fe, HBV_{\beta} - fe, HBV_{\alpha}$	(5)	
LISFLOODFP-MEAS: $fe, G(\alpha, \beta) = fe, G_{\beta} - fe, G_{\alpha}$	(6)	$fe, HBV_i$ = monthly maximum floodplain inundation extent predicted by LISFLOODFP-HBV for month $i$
<ul style="list-style-type: none"> <li>Volume and flood extent differences</li> </ul>		
Input volume:		
$\Delta iv(\alpha, \beta) = iv, HBV(\alpha, \beta) - iv, G(\alpha, \beta)$	(7)	$fe, G_i$ = monthly maximum floodplain inundation extent predicted by LISFLOODFP-MEAS for month $i$
Floodplain inundation volume:		
$\Delta fv(\alpha, \beta) = fv, HBV(\alpha, \beta) - fv, G(\alpha, \beta)$	(8)	
Floodplain inundation extent:		
$\Delta fe(\alpha, \beta) = fe, HBV(\alpha, \beta) - fe, G(\alpha, \beta)$	(9)	$\alpha$ = first month (day) of the evaluation period $\beta$ = last month (day) of the evaluation period
<ul style="list-style-type: none"> <li>Performance metrics for the continuous simulation analysis</li> </ul>		
Root mean square deviation: $RMSD = \sqrt{\frac{\sum_{i=1}^M (sim_i - meas_i)^2}{M}}$	(10)	$sim_i = \begin{cases} hbv_i \\ iv, HBV(1, i) \\ fv, HBV(1, i) \\ fe, HBV(1, i) \end{cases}$
Percent bias: $PBIAS = 100 * \frac{\sum_{i=1}^M (sim_i - meas_i)}{\sum_{i=1}^M meas_i}$	(11)	
Nash-Sutcliffe: $NS = 1 - \frac{\sum_{i=1}^M (meas_i - sim_i)^2}{\sum_{i=1}^M (meas_i - \overline{meas})^2}$ , $\overline{meas} = \frac{\sum_{i=1}^M meas_i}{M}$	(12)	
R-squared: $R^2 = 1 - \frac{\sum_{i=1}^M (meas_i - \hat{sim}_i)^2}{\sum_{i=1}^M (meas_i - \overline{meas})^2}$ , $\hat{sim}_i = a * sim_i + b$	(13)	$meas_i = \begin{cases} g_i \\ iv, G(1, i) \\ fv, G(1, i) \\ fe, G(1, i) \end{cases}$ $M$ = total number of months (days) used in the numerical experiment (e.g., $M = 84$ months)
$a$ and $b$ are the coefficients of the linear regression		
<ul style="list-style-type: none"> <li>Performance metrics used in the event-based time series analysis</li> </ul>		
Inputs ratio: $IR = \frac{iv, HBV(\alpha=start, \beta=end)}{iv, G(\alpha=start, \beta=end)}$	(14)	$\alpha = start$ : starting month of the low-/high-flow period
Volumes difference ratio: $VDR = \frac{\Delta fv(\alpha=start, \beta=end)}{\Delta iv(\alpha=start, \beta=end)}$	(15)	$\beta = end$ : end month of the low-/high-flow period
Peaks ratio: $PR = \frac{\max(iv, HBV(\alpha=start, \beta=end))}{\max(iv, G(\alpha=start, \beta=end))}$	(16)	

modeling framework at the large scale. In this study, HBV-simulated daily discharge values were used as input to the hydraulic model LISFLOOD-FP for the prediction of floodplain inundation volumes and extents in the MDB from 1 January 2006 to 31 December 2012. This model setup will hereafter be referred to as LISFLOODFP-HBV. Measured daily discharge values for the same 7-year period were then used as input to LISFLOOD-FP to produce benchmark predictions of floodplain inundation dynamics. This latter model setup will thereafter be referred to as LISFLOODFP-MEAS. Missing data in measured time series were replaced with HBV-simulated flows. Simulated and measured discharge time series of gauge stations located along the same river were edited to avoid double counting of inflow volumes.

It is here noted that the simulation period of the hydraulic model was the same as the calibration period of the hydrologic model (section 3.1). Although hydrological models calibrated over a historical period are often used in a forecasting framework, the dependence of the optimal parameter set on the climate characteristics of the calibration period and the challenges of the transferability of these parameters to forecasting scenarios have been previously demonstrated (Brigode et al., 2013; Romanowicz & Booij, 2015; Vaze et al., 2010). Consequently, in this experimental design, discrepancies between modeled and measured discharge hydrographs were expected to be lower than in a real forecasting scenario. Moreover, as explained above, the

correction of the missing data in the measured time series further reduced the difference between simulated and measured discharge time series. For these reasons, this study had the merit to allow the investigation of the impact of relatively small input discrepancies in the prediction of floodplain inundation volumes and extents.

Monthly maximum values of floodplain inundation volumes and extent predicted by LISFLOODFP-HBV (i.e., using modeled streamflow; thereafter indicated with  $f_v, HBV_i$  and  $f_e, HBV_i$  as explained in Table 1) and LISFLOODFP-MEAS (i.e., using gauged streamflow; thereafter indicated with  $f_v, G_i$  and  $f_e, G_i$  as explained in Table 1) were compared by counting the number of flooded cells in the floodplain (i.e., river cells were omitted). A cell in the floodplain was flagged as flooded if the computed water depth was higher than 5 cm; a sensitivity analysis not shown in this paper demonstrated that the use of a different threshold value (1, 10, and 50 cm) did not affect the outcomes of the analysis presented thereafter, attributed to the inherently large vertical error variations in the SRTM topography (a discussion of these errors can be found in Domeneghetti, 2016). Discrepancies between simulated and measured cumulative input volumes (equations 1 and 2 in Table 1) over a lapse of time could lead to discrepancies in the prediction of floodplain dynamics. Increments of monthly maximum values of floodplain inundation volumes and extent (equations 3 to 6 in Table 1) were computed to evaluate the cumulative effect of discrepancies in input data. Input volumes and inundation volumes were measured in cubic kilometer, and inundation extents were reported as the number of cells. Inundation areas can be obtained by multiplying the number of cells by the square value of the hydraulic model cell size (i.e., 1 km<sup>2</sup>); in this paper, the choice of reporting the number of cells allowed a holistic understanding of the interactions between input discrepancies and model resolution and thus their impact on predicted inundation dynamics.

### 3.3.1. Basin Hierarchy Approach

The analysis was performed using a basin hierarchy approach. More specifically, the analysis first focused on the upstream subcatchments, where inundation extents and volumes are caused by discharge time series of input points located within the same subcatchment area. These upstream subcatchments are hydrologically independent and represent level 1 of the basin hierarchy approach introduced here. Moving from upstream to downstream, the aggregation of a number of upstream, hydrologically independent subcatchments of level 1 allowed the analysis of larger areas. In these areas, inundation extents and volumes are caused by the combination of discharge hydrographs of input points located within the area itself and the routing of discharge hydrographs introduced in upstream (level 1) areas. These clusters represent level 2 of the hierarchy approach. Level 3 is defined by the aggregation of level 2 clusters, allowing the analysis of inundation extents and volumes in downstream areas, which are often far from the input points. This aggregation strategy is repeated until inclusion of the total basin area. Consequently, the number of levels required by this approach depends on the morphology of the basin under investigation.

In this study, the 28 HRR (Figure 1b) were modified and aggregated to first delineate hydrologically independent subcatchments of level 1 and then define the aggregated subcatchments clusters of levels 2–4. Huang et al. (2013) previously used inundation extents derived from remote sensing (Landsat) images and a DEM to edit the boundaries of the HRR in order to generate ecohydrological zones with enhanced flow connectivity. A similar aim was pursued here by using a pragmatic approach based on flow path connectivity, as shown by the results of the hydraulic model. More specifically, outputs of the hydraulic model were used for the definition of the aggregated areas, allowing correct inclusion of inundated areas from a set of input flow hydrographs. For this reason, as seen in Figure 1b, lines representing the downstream boundary of the investigated area for different basin hierarchy levels do not often coincide with the boundaries of the HRR. Level 1 hydrologically independent areas are often the upstream area of the HRR. Level 2 clusters are (i) the South cluster (S), including the subcatchments contributing to the Murrumbidgee River; (ii) the North-West cluster (NW), including the Paroo and Warrego Rivers; and (iii) the North-East cluster (NE), including the subcatchments contributing to the Balonne-Bokhara-Narran Rivers. Level 3 is the union of the level 2 clusters and downstream HRR; more specifically, level 3 clusters are the Centre-North (CN) and Centre-South (CS) clusters. The allocation of level 1 areas to level 2 and level 3 clusters is also listed in Table S1 (supporting information). Level 4 fully encompasses the MDB.

### 3.3.2. Continuous Simulation Analysis

For each level, aggregated simulated and measured input discharge time series were computed by adding the time series of all the input points affecting the area of interest from 1 January 2006 to 31 December 2012,

according to the spatial subdivision described in section 3.3.1. Simulated daily, monthly, and cumulative time series of input volumes ( $hbv_i$ ;  $iv,HBV$  as in Table 1) were compared with measured daily, monthly, and cumulative time series ( $g_i$ ;  $iv,G$  as in Table 1) by computing the *RMSD*, percent bias (*PBIAS*), *NS*, *R*-squared ( $R^2$ ) according to equations 10 to 13 in Table 1. The same statistics were used to compare time series of monthly maximum inundation volumes and extents computed by LISFLOODFP-HBV with the results of LISFLOODFP-MEAS; the latter results were used as a benchmark. The *RMSD* and *PBIAS* values provide information on the magnitude and sign of the discrepancy between simulation-based and measurement-based results and are discussed in detail in the paper. The values of *NS* and  $R^2$  allow a more comprehensive analysis of the results and are listed in the supporting information (Tables S1–S3).

The statistics of equations 10 to 13 were complemented by a comparison between the cumulative input volumes and the floodplain inundation volumes and extents evaluated at the end of the 7-year simulation period. More specifically, the difference between the cumulative simulated and measured input volumes  $\Delta iv(\alpha = 1, \beta = 84)$  (equation 7, Table 1) at the end of the 7-year simulation period was compared to the difference between the LISFLOODFP-HBV- and LISFLOODFP-MEAS-predicted monthly maximum floodplain inundation volumes  $\Delta fv(\alpha = 1, \beta = 84)$  and extents  $\Delta fe(\alpha = 1, \beta = 84)$  (equations 8 and 9, Table 1) at the end of the 7-year simulation period (84 months). This analysis was included in the assessment of the continuous modeling approach as it allows comparing the difference between input volumes with the difference between floodplain inundation volume and extent at the end of the study period. Albeit limited to a 7-year time period, it was assumed that this analysis allowed an insight on the long-term response of the hydraulic model to discrepancies in discharge input data.

### 3.3.3. Event-Based Time Series Analysis

An event-based analysis allowed investigation of the behavior of the models during low-flow and high-flow periods. Low- and high-flow periods were defined based on cumulative values of measured input volumes using a simple but automatic algorithm. The algorithm computed the average monthly input volume  $V_m$  for the full time series (2006–2012; i.e., total input volume/total number of months). Months having an input volume smaller than  $V_m$  belonged to low-flow periods; months having an input volume larger than  $V_m$  belonged to high-flow periods. The largest monthly input volume was used to identify large high-flow periods; remaining high-flow periods were classified as small to moderate high-flow periods. Each low- and high-flow period was isolated from the full time series, and the analysis of impacts of discrepancies in the input data on the modeled inundation extent and volumes was achieved by computing the indices inputs ratio (*IR*), volumes difference ratio (*VDR*), and Peaks Ratio (*PR*) according to equations 14 to 16 in Table 1.

More specifically, for each low- or high-flow period, *IR* is the ratio of simulated to measured input volume, meaning that *IR* is higher than 1 when the hydrological model overestimates the measured discharge data and lower than 1 for underestimation. *VDR* is the ratio of the difference of the monthly maximum floodplain inundation volumes predicted by LISFLOODFP-HBV and LISFLOODFP-MEAS to the difference of the simulated and measured input volumes. These differences are the increments from the start to end of the selected period (equations 8 and 7 in Table 1). *VDR* is positive when the largest input time series leads to the largest inundation volume; it is negative when the smallest input time series leads to the largest inundation volume. Moreover, absolute values of *VDR* larger than 1 indicate that the hydraulic model exacerbates the difference between the input time series. It is noted here that a theoretically perfect hydrological model would lead to a zero denominator in equation 15. However, such a condition did not occur in this analysis. *IR* and *VDR* were evaluated from the start to end of each selected low- or high-flow period. *PR* was computed only for high-flow periods and it is defined as the ratio of the simulated input flood peak to the measured input flood peak.

Finally,  $\Delta fv(\alpha, endLHF)$  and  $\Delta fe(\alpha, endLHF)$  are the difference between monthly maximum floodplain inundation volumes and extents predicted by LISFLOODFP-HBV and LISFLOODFP-MEAS during large high flows (LHF; equations 8 and 9 in Table 1). These differences were defined in two different ways to analyze the outcomes of a continuous modeling approach as opposed to an event-based modeling approach. In detail, equations 8 and 9 were solved with  $\alpha = 1$  to analyze the outcomes of a continuous modeling approach. In this case, LISFLOODFP-HBV and LISFLOODFP-MEAS inundation volumes and extents were retrieved at a snapshot in time and represented the cumulative maximum floodwater expansion after the investigated flood event. Conversely, when exploring the outcomes of an event-based modeling approach, equations 8

and 9 were solved with  $\alpha = \text{startLHF}$ ; that is, LISFLOODFP-HBV and LISFLOODFP-MEAS inundation volumes and extents were computed as increments from the start to end of the flood event. A schematic of this is shown in Figure 2a.

## 4. Results

### 4.1. Hydrologically Independent Subcatchments (Level 1)

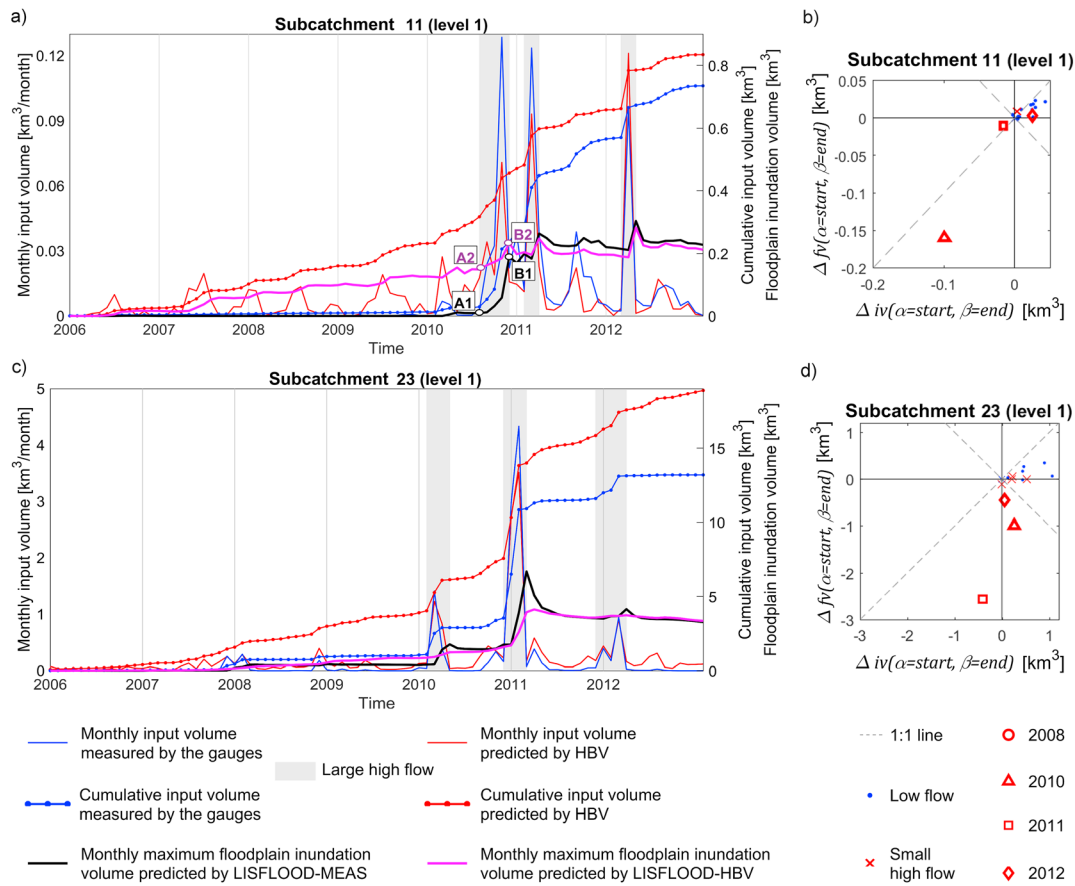
#### 4.1.1. Continuous Simulation Analysis

Table 2 lists mean and median values of the statistics of equations 10 and 11 computed for all of the hydrologically independent subcatchments of level 1. The statistics of equations 10 to 14 for each hydrologically independent subcatchment are reported in Table S1 (supporting information). As anticipated in section 3.1, HBV-simulated discharge values could adequately reproduce the hydrological variability of the MDB. The median *RMSD* values for daily and cumulative time series of input volumes were 0.001 and 0.305 km<sup>3</sup>, respectively. The *RMSD* values of the floodplain inundation volumes were generally lower than the *RMSD* values of the cumulative volume inputs (median *RMSD* of floodplain inundation volumes was 0.052 km<sup>3</sup>). The high values of the *NS* and *R*<sup>2</sup> of the time series of floodplain inundation volumes and extents (median values were 0.78 and 0.92 for the *NS* and 0.80 and 0.89 for *R*<sup>2</sup>, respectively) highlighted a good overall agreement between the outcomes of LISFLOODFP-HBV and LISFLOODFP-MEAS (Table S1). The *PBIAS* of the floodplain inundation volumes and extents predicted by LISFLOODFP-HBV and LISFLOODFP-MEAS were consistently lower than the *PBIAS* of the cumulative volume input data (median values were 33 and 17 for floodplain inundation volumes and extent, respectively, and 57 for the cumulative input volume). These results suggested that flood wave routing could (at least) partially mask differences in the input time series.

However, the MDB has a large morphological and hydrological variability, and different patterns in subcatchment behaviors were identified. Discrepancies between simulated and measured discharge time series were small in a number of subcatchments (e.g., 1, 2, 5, 12, and 19), thus leading to negligible discrepancies in predicted floodplain inundation volumes and extents (Table S1). Conversely, some subcatchments (e.g., 3, 5, 13, 15, 23, and 24) resulted in negative values of *PBIAS* and low values of *NS* of the predicted time series of monthly maximum inundation volumes and extent (Tables 2 and S1). Moreover, despite the total difference  $\Delta \text{in}(\alpha = 1, \beta = 84)$  between cumulative values of simulated and measured input volumes being positive for all the subcatchments, the difference  $\Delta \text{in}(\alpha = 1, \beta = 84)$  between floodplain inundation volumes predicted by LISFLOODFP-HBV and LISFLOODFP-MEAS was negative for 11 out of 19 subcatchments (as shown by the results for subcatchment 11, by the mean and median values in Tables 2 and S1). These negative values indicated that despite LISFLOODFP-HBV being forced with higher total input volumes, it resulted in smaller total inundation volumes than did LISFLOODFP-MEAS. The understanding of these results was achieved with an in-depth event-based analysis.

#### 4.1.2. Event-Based Time Series Analysis

As explained in section 2, years 2006 to 2009 were generally characterized by low-flow conditions with some small to moderate high-flow periods (2008), while large high flows occurred in 2010, 2011, and 2012. An extensive effort for the identification of patterns in the response of floodplain inundation dynamics to discrepancies in input data during low- and high-flow periods led to the identification of two representative subcatchments, namely, subcatchment 11 and subcatchment 23. More specifically, subcatchment 11 belongs to the southern area of the MDB, while subcatchment 23 belongs to the northern area of the MDB. Results for these subcatchments are presented into detail thereafter, and a list of subcatchments having similar behaviors is provided. Table 3 shows the values of the performance metrics of equations 8, 9, 14, to 16 computed for subcatchments 11 and 23 and the mean and median values of all of the level 1 subcatchments. The results for each hydrologically independent subcatchment are reported in Table S2 (supporting information). Figures 2a and 2c show the time series of simulated and measured discharge data (monthly values and cumulative values) as well as floodplain monthly maximum inundation volumes predicted by LISFLOODFP-HBV and LISFLOODFP-MEAS for subcatchments 11 and 23. In the MDB, measured discharge during low flows is almost negligible compared to high flows, and the maximum monthly inundation volumes and extents are the outcome of the total amount of discharge cumulated over high-flow days. Consequently, use of input monthly values in Figures 2a and 2c (and subsequently in Figures 4a, 4c, 4e,



**Figure 2.** Analysis of level 1 areas. (a, c) Time series of gauged and modeled input volumes (monthly and cumulative values) and monthly maximum floodplain inundation volumes predicted by LISLOODFP-MEAS and LISLOODFP-HBV;  $\Delta iv(1, endLHF) = B2 - B1$  and  $\Delta iv(startLHF, endLHF) = (B2 - A2) - (B1 - A1)$ . (b, d) Event-based comparison of differences of input volumes and differences of monthly maximum floodplain inundation volumes;  $\Delta iv(\alpha = start, \beta = end)$  and  $\Delta iv(\alpha = start, \beta = end)$ , as defined in Table 1, equations 7 and 8, respectively. (a, b) Level 1 subcatchment 11. (c, d) Level 1 subcatchment 23.

and 5a) allowed a straightforward visualization of the relationship between inputs and maximum inundation volumes.

#### 4.1.2.1. Low-flow periods

As shown in Tables 3 and S2, during low-flow periods the simulated discharge values were higher than the measurements with *IR* consistently higher than 1. The discrepancies in input volumes were reduced by the flow routing and *VDR* was slightly higher than 0, indicating that the inundation volumes predicted by LISLOODFP-HBV were slightly larger than the values predicted by LISLOODFP-MEAS. This result

**Table 2**  
Continuous Time Series Analysis of Hydrologically Independent Subcatchments (Level 1)

Subcatchment	Daily input volume		Cumulative input volume			Floodplain inundation volume			Floodplain inundation extent		
	<i>RMSD</i> (km <sup>3</sup> )	<i>PBIAS</i> (%)	<i>RMSD</i> (km <sup>3</sup> )	<i>PBIAS</i> (%)	$\Delta iv(1,84)$ (km <sup>3</sup> )	<i>RMSD</i> (km <sup>3</sup> )	<i>PBIAS</i> (%)	$\Delta fv(1,84)$ (km <sup>3</sup> )	<i>RMSD</i> (Cells n.)	<i>PBIAS</i> (%)	$\Delta fe(1,84)$ (Cells n.)
11	0.001	13.4	0.144	65.9	0.099	0.074	61.1	-0.016	52	48.0	-5
23	0.011	43.2	2.954	57.3	5.699	0.395	-1.1	0.080	123	1.4	7
Mean level 1	0.003	40.1	0.512	69.4	0.746	0.093	26.1	-0.001	40	23.2	3
Median level 1	0.001	28.0	0.305	57.3	0.316	0.052	32.9	-0.001	18	16.5	-5

*Note.* *RMSD* = root mean square deviation as in equation 10. *PBIAS* = percent bias as in equation 11.  $\Delta iv(1, 84)$  = difference between simulated and measured cumulative input volume as in equation 7.  $\Delta fv(1, 84)$  and  $\Delta fe(1, 84)$  = difference between the LISLOODFP-HBV- and LISLOODFP-MEAS-predicted floodplain inundation volumes and extents as in equations 8 and 9, respectively. All the differences were evaluated at the end of the investigated time series (i.e., 84 months). Cells n. = number of flooded cells.

**Table 3**  
Event-Based Analysis of Hydrologically Independent Subcatchments (Level 1)

Subcatchment	Low flows		Small high flows			Large high flows			$\Delta f_v(\alpha, \text{endLHF})$ (km <sup>3</sup> )		$\Delta f_e(\alpha, \text{endLHF})$ (Cells n.)	
	<i>IR</i>	<i>VDR</i>	<i>IR</i>	<i>PR</i>	<i>VDR</i>	<i>IR</i>	<i>PR</i>	<i>VDR</i>	$\alpha = 1$	$\alpha = \text{startLHF}$	$\alpha = 1$	$\alpha = \text{startLHF}$
11	25.62	0.59	0.96	0.88	1.67	0.77	0.73	1.61	0.043	−0.094	78	−18
23	14.12	0.27	1.09	0.91	−5.10	0.95	0.81	6.08	−2.749	−2.560	−605	−494
Mean level 1	9.57	0.21	1.18	0.88	−1.34	0.83	0.68	0.42	−0.180	−0.245	−3	−108
Median level 1	7.06	0.16	1.07	0.89	−0.81	0.8	0.68	0.55	−0.005	−0.065	−12	−31

Note. *IR* = inputs ratio as in equation 14. *VDR* = volumes difference ratio as in equation 15. *PR* = peaks ratio as in equation 16.  $\Delta f_v(\alpha, \text{endLHF})$  and  $\Delta f_e(\alpha, \text{endLHF})$  = difference between the LISFLOODFP-HBV- and LISFLOODFP-MEAS-predicted floodplain inundation volumes and extents for large high flows as in equations 8 and 9, respectively. Here,  $\Delta f_v(\alpha, \text{endLHF})$  and  $\Delta f_e(\alpha, \text{endLHF})$  values are for the largest flood event. Cells n. = number of flooded cells.

was observed in all the level 1 subcatchments, and it is also shown by the first quadrants of Figures 2b and 2d, where all the points are below the 1:1 line.

#### 4.1.2.2. Moderate high-flow periods

During moderate high-flow periods *IR* was generally higher than 1; however, *VDR* was often negative, indicating that LISFLOODFP-HBV predicted smaller inundation volumes than did LISFLOODFP-MEAS. This counterintuitive outcome can be explained by the impact of flood peak values on the modeled inundation volumes and extents. In these events, simulated input volumes were larger than measured values, but the simulated flood peaks were lower than the observations, and *PR* was lower than 1. Lower simulated flood peaks resulted in limited overflow from the main river to the floodplain and across the floodplain cells when using LISFLOODFP-HBV. Examples are the 2010 and 2012 flood events in subcatchment 23 as shown in the second quadrant of Figure 2d (triangle and diamond symbols, respectively).

#### 4.1.2.3. Large high-flow periods

For large high flows, simulated input volumes and peak flows were lower than the measured values (*IR* < 1 and *PR* < 1), and consequently, LISFLOODFP-HBV predicted lower inundation volumes and extents than did LISFLOODFP-MEAS (*VDR* > 0). In fact, absolute values of *VDR* were often higher than 1 (Tables 3 and S2), indicating that flood wave routing exacerbated the differences in input volumes. As a result, it can be inferred that large measured flood peaks triggered extensive overflow from the river to the floodplain and across the floodplain cells. Conversely, similarly extensive floodplain inundation was not achieved by lower simulated flood peaks. This pattern can be clearly seen in the third quadrant of Figures 2b and 2d, where the triangle representing the 2010 flood in subcatchment 11 and the square representing the 2011 flood in subcatchment 23 are on the right side of the 1:1 line. In particular, in subcatchment 23, 2011 pre-flood inundation volumes were similar for both LISFLOODFP-HBV and LISFLOODFP-MEAS (Figure 2c). Compared with LISFLOODFP-HBV, LISFLOODFP-MEAS was forced by a larger flood peak, which, combined with the specific morphology of the area, resulted in the flooding of a larger number of cells. In fact, in this area, a natural restriction (called the Barrackdale choke) exacerbated the impact of the underestimation of flood peak values, causing a large discrepancy between inundation volumes predicted by LISFLOODFP-HBV and LISFLOODFP-MEAS (Figure 3a).

### 4.1.3. Interactions Between Low- and High-Flow Periods

#### 4.1.3.1. Low-flow periods impact on high-flow periods

In a continuous modeling approach, pre-flood inundation conditions sensibly affected the discrepancies between LISFLOODFP-HBV and LISFLOODFP-MEAS for large flood events. More specifically, *IR* values higher than 1 and positive, yet low *VDR* values, during the low-flow periods led to a progressive and steady expansion of inundation volumes and extents predicted by LISFLOODFP-HBV as opposed to the nearly zero values predicted by LISFLOODFP-MEAS. Consequently, in a continuous modeling approach, overestimation of measured discharge values during low-flow periods masked the differences in the prediction of inundation volumes during high-flow periods. This impact was observed in 15 hydrologically independent subcatchments (specifically, subcatchments 1, 2, 5, 6, 7, 8, 9, 11, 12, 13, 17, 19, 20, 21, and 24; Table S2). A representative case is the 2010 flood in subcatchment 11 (Figure 2a, Table 3) for which  $\Delta f_v(\alpha, \text{endLHF})$  between increments of inundation volumes predicted by LISFLOODFP-HBV and LISFLOODFP-MEAS were 0.043 km<sup>3</sup> in a continuous modeling approach ( $\alpha = 1$ ) and −0.094 km<sup>3</sup> in an event-based modeling approach ( $\alpha = \text{startLHF}$ ).

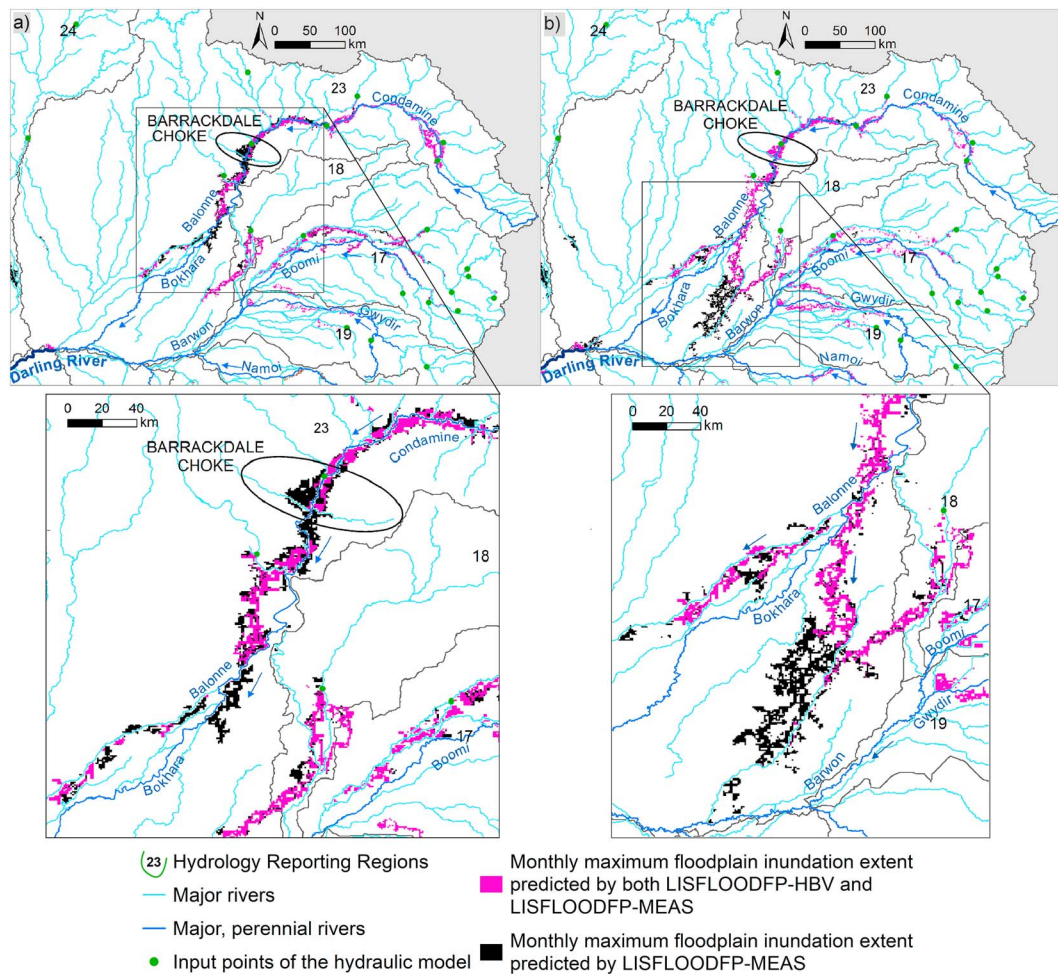


**Figure 3.** Modeled monthly maximum inundation extent in the North-East area of the Murray Darling Basin (a) after the 2011 flood event (February) and (b) after the 2012 flood event (April). Location of the Barrackdale Choke (black oval) and downstream boundary of level 1 subcatchment 23 (green line) are also shown. The close-up insets show the discrepancies between LISFLOOD-HBV and LISFLOOD-MEAS.

#### 4.1.3.2. High-flow periods impact on low-flow periods

The event-based analysis could explain negative *PBIAS* and *NS* values for continuous time series of inundation volumes previously mentioned for some of the hydrologically independent subcatchments (specifically, subcatchments 3, 5, 13, 15, and 23, as shown in Tables 2 and S1). In these subcatchments, simulated input volume and flood peak values were lower than the measured values for a sequence of high-flow events. Consequently, LISFLOODFP-HBV predicted lower inundation values than did LISFLOODFP-MEAS. This negative difference increased with time and affected most of the analyzed time series, thus resulting in the negative *PBIAS* and *NS* values shown in the continuous time series analysis.

### 4.2. Catchment Clusters

#### 4.2.1. Level 2: South, North-West, and North-East Clusters

In level 2 clusters, simulated and measured input volume time series had a good overall agreement, as demonstrated by the relatively low values of the *RMSD* listed in Table 4 and the relatively high values of the *NS* and *R<sup>2</sup>* reported in Table S3 (supporting information). However, the *PBIAS* of the input volume time series had the opposite sign of the *PBIAS* of monthly maximum inundation volumes and extents with LISFLOODFP-HBV predicting lower inundation volumes and extents than those by LISFLOODFP-MEAS at the end of the modeling period (i.e.,  $\Delta f_v(1,84)$  and  $\Delta f_e(1,84)$  had negative values, as shown in Table 4). This result is also shown in Figures 4a, 4c, and 4e, with Table 5 listing the results of the analysis of low- and high-flow periods. In each cluster, and consistently with the results of the hydrologically independent

**Table 4**  
Continuous Time Series Analysis of Level 2 and Level 3 Clusters

Cluster	Daily input volume		Cumulative input volume			Inundation volume			Inundation extent		
	RMSD (km <sup>3</sup> )	PBIAS (%)	RMSD (km <sup>3</sup> )	PBIAS (%)	$\Delta iv(1,84)$ (km <sup>3</sup> )	RMSD (km <sup>3</sup> )	PBIAS (%)	$\Delta iv(1,84)$ (km <sup>3</sup> )	RMSD (Cells n.)	PBIAS (%)	$\Delta fe(1,84)$ (Cells n.)
S	0.124	6.8	2.334	20.6	1.929	0.998	-30.4	-2.652	956	-38.3	-2,381
NE	0.185	34.1	3.356	48.9	6.136	0.566	-16.5	-0.408	417	-19.0	-242
NW	0.102	34.4	1.918	25.6	4.109	0.441	-58.5	-0.689	521	-61.4	-381
CN3	0.300	34.0	7.633	42.2	14.264	1.460	-28.0	-1.819	997	-26.2	-1,146

Note. RMSD = root mean square deviation as in equation 10. PBIAS = percent bias as in equation 11.  $\Delta iv(1,84)$  = difference between simulated and measured cumulative input volume as in equation 7.  $\Delta iv(1,84)$  and  $\Delta fe(1,84)$  = difference between the LISFLOODFP-HBV- and LISFLOODFP-MEAS-predicted floodplain inundation volumes and extents as in equations 8 and 9, respectively. All the differences were evaluated at the end of the investigated time series (i.e., 84 months). Cells n. = number of flooded cells. S = South; NE = North-East; NW = North-West; CN3 = Centre-North, level 3.

subcatchments, low-flow periods were characterized by *IR* values larger than 1 and *VDR* positive, but close to 0 values, highlighting that inundation volumes discrepancies were smaller than input volumes discrepancies (as shown in the first quadrant of Figures 4b, 4d, and 4f where most of the points are below the 1:1 line). In moderate and large high-flow periods, simulated flood peak values lower than observations (with *PR* lower than 1) enhanced the negative difference between inundation volumes predicted by LISFLOODFP-HBV and LISFLOODFP-MEAS, even when *IR* was larger than 1 as for the 2010 event in North-East cluster (Figures 4c and 4d, and Table 5). In the South cluster, the impact of simulated flood peak values lower than observations was exacerbated by the low accuracy of the SRTM, which hindered floodplain drainage in low-slope areas, and the difference between LISFLOODFP-HBV and LISFLOODFP-MEAS increased after each large flood event in 2010, 2011, and 2012 (Figure 4a and Table 5).

In the North-East cluster, the inundation volume and extent during the 2011 flood event were highly affected by the different results of LISFLOODFP-HBV and LISFLOODFP-MEAS for subcatchment 23 (section 4.1.2 and Figures 2c, 2d, and 3a). Flood wave routing predicted by LISFLOODFP-HBV could not trigger any flooding downstream of the Barrackdale Choke. Conversely, LISFLOODFP-MEAS predicted extensive floodplain inundation up to the confluence with the Bokhara River (Figure 3a). Large inundated areas in 2011 were quickly reactivated in 2012, and differences between LISFLOODFP-HBV and LISFLOODFP-MEAS increased over time in the nearly flat area between the Bokhara and Barwon Rivers (Figure 3b).

In the North-West cluster, large flood events in 2010 and 2012 offered a peculiar case study within the database analyzed here. Simulated input volumes and flood peak values were larger than the measured data (*IR* > 1 and *PR* > 1). Nevertheless, LISFLOODFP-HBV predicted smaller inundation volumes than did LISFLOODFP-MEAS (*VDR* < -1; Figure 4f, second quadrant). Analysis of the number of flooded cells allowed the understanding of this result. During the large 2008 flood, the simulated discharge hydrograph triggered the flooding of a small number of cells in HRR 24 and 25 (location of these HRR can be seen in Figure 1b) when compared to the results of LISFLOODFP-MEAS (Figure 4e; negative *PBIAS* of modeled inundation extents for catchment 24 in Table S1). Despite partial drainage of inundated areas, LISFLOODFP-MEAS reached conditions of incipient flooding, and most of the formerly flooded cells were reactivated during the subsequent flood events, thus contributing to total flood inundation extents and volumes larger than those of LISFLOODFP-HBV.

In all the clusters, interaction between the morphological features and flashy characteristics of the flood hydrographs resulted in large differences between LISFLOODFP-HBV and LISFLOODFP-MEAS. These differences increased over time when using a continuous modeling approach. Conversely, differences between LISFLOODFP-HBV and LISFLOODFP-MEAS were less severe when using an event-based approach (Table 5). For example, in the North-East cluster, differences between inundation volumes  $\Delta iv(\alpha, endLHF)$  and extents  $\Delta fe(\alpha, endLHF)$  for the 2012 flood were -1.20 km<sup>3</sup> and -1,116 cells when using a continuous modeling approach ( $\alpha = 1$ ) but only -0.52 km<sup>3</sup> and -661 cells when using an event-based modeling approach ( $\alpha = startLHF$ ).

#### 4.2.2. Level 3 and Level 4 Clusters

Flooding in the Centre-North cluster (level 3) of the MDB (Figure 1b) was driven by the North-West cluster in 2008, 2010, and 2012 and by the North-East cluster in 2011. Differences between LISFLOODFP-HBV and

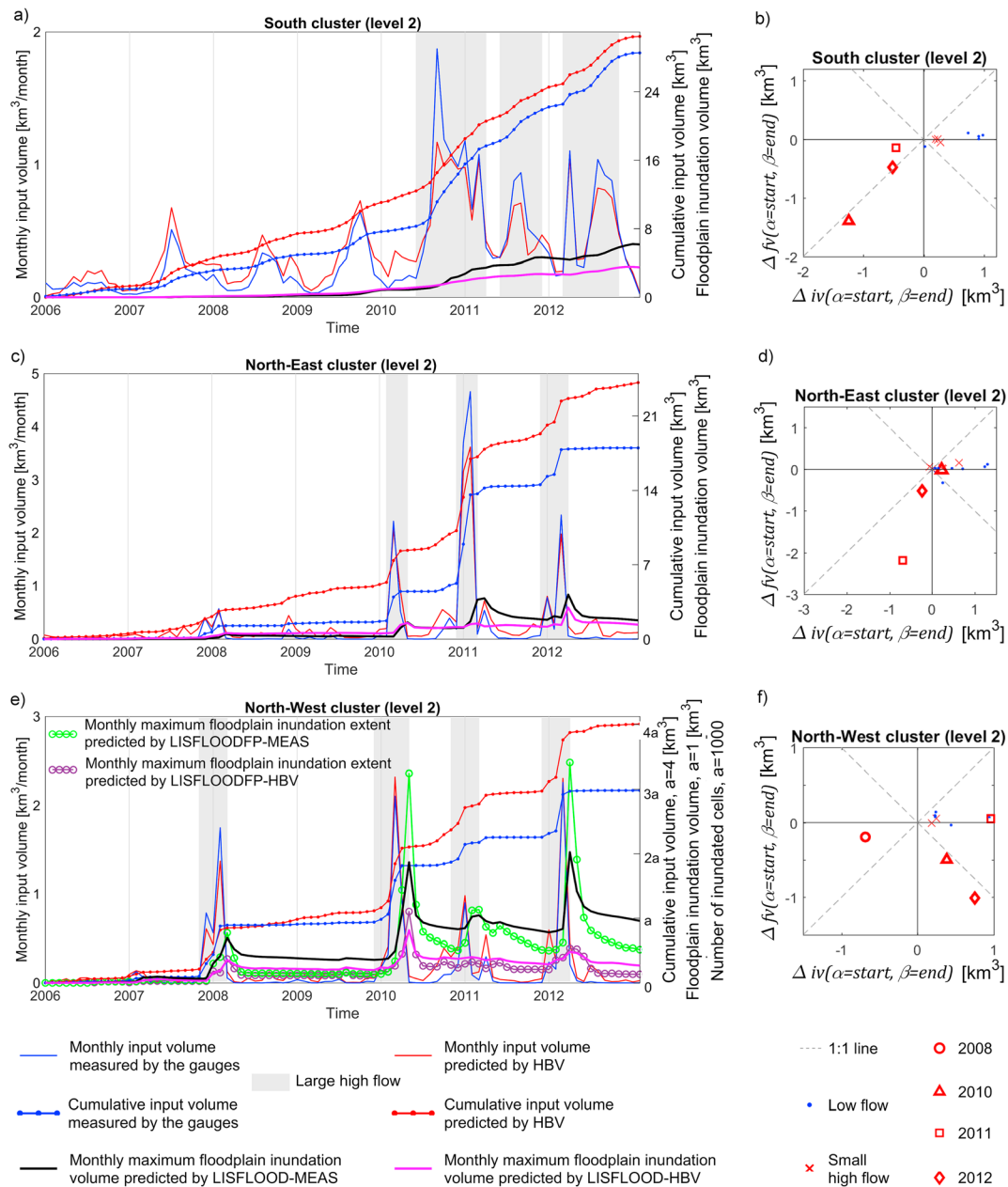


**Figure 4.** Analysis of level 2 clusters. (a, c, e) Time series of gauged and modeled input volumes (monthly and cumulative values) and monthly maximum floodplain inundation volumes predicted by LISFLOODFP-MEAS and LISFLOODFP-HBV. (b, d, f) Event-based comparison of differences of input volumes and differences of monthly maximum floodplain inundation volumes;  $\Delta iv(\alpha = start, \beta = end)$  and  $\Delta fv(\alpha = start, \beta = end)$  as defined in Table 1, equation 7 and 8, respectively. (a, b) South cluster; (c, d) North-East cluster; and (d, e) North-West cluster.

LISFLOODFP-MEAS were small in 2008 and 2010 (Figure 5a and  $VDR \sim 0$  in Table 5). In 2011, morphological features loosely described by the SRTM combined with the flashy hydrological regime led to flood inundation volume discrepancies larger than the discrepancies in input discharge hydrographs. The simulated flood peak and total input volume in 2011 were lower than the observations ( $PR = 0.77$  and  $IR = 0.91$ ). LISFLOODFP-HBV predicted a sensibly lower inundation volume than did LISFLOODFP-MEAS with a  $VDR$  of 1.37 (Figure 5b, square symbol in the third quadrant). These results show that discrepancies detected for the level 2 clusters did not fade when analyzing larger downstream areas. In fact, the disagreement between LISFLOODFP-HBV and LISFLOODFP-MEAS increased over time and was moving in the downstream direction. In other words, flood wave routing exacerbated the

**Table 5**  
Event-Based Analysis of Level 2 and Level 3 Clusters

Cluster	Low flows		Small high flows			Large high flows			$\Delta fv(\alpha, endLHF)$ (km <sup>3</sup> )		$\Delta fe(\alpha, endLHF)$ (Cells n.)		
	IR	VDR	IR	PR	VDR	Year	IR	PR	VDR	$\alpha = 1$	$\alpha = startLHF$	$\alpha = 1$	$\alpha = startLHF$
S	1.67	0.03	1.28	1.37	0.33	2011	0.87	0.63	1.20	-1.181	-1.392	-1,245	-1,383
						2012	0.86	0.79	1.01	-2.331	-0.473	-2,157	-583
NE	9.91	0.51	1.95	1.51	0.08	2010	1.08	0.93	-0.06	0.297	-0.013	-17	-150
						2011	0.92	0.78	3.18	-2.214	-2.186	-1,271	-1,246
						2012	0.93	0.85	2.21	-1.196	-0.517	-1,116	-661
NW	7.00	0.07	1.10	1.07	0.01	2008	0.78	0.78	0.28	-0.226	-0.193	-240	-232
						2010	1.11	1.10	-1.32	-0.665	-0.507	-989	-975
						2011	1.73	1.09	0.06	-0.458	0.061	-324	124
						2012	1.26	1.02	-1.38	-1.543	-1.039	-2,876	-2,575
CN3	3.90	0.06	1.10	0.95	0.27	2008	0.94	0.85	0.50	-0.063	-0.148	-281	-381
						2010	1.26	1.06	-0.01	0.385	-0.017	189	82
						2011	0.91	0.77	1.37	-2.774	-3.044	-2,758	-2,895
						2012	1.11	0.96	-1.17	-3.776	-1.007	-3,054	-1,187

Note. IR = inputs ratio as in equation 14. VDR = volumes difference ratio as in equation 15. PR = peaks ratio as in equation 16.  $\Delta fv(\alpha, endLHF)$  and  $\Delta fe(\alpha, endLHF)$  = difference between the LISFLOODFP-HBV- and LISFLOODFP-MEAS-predicted floodplain inundation volumes and extents for large high flows as in equations 8 and 9, respectively. Cells n. = number of flooded cells. S = South; NE = North-East; NW = North-West; CN3 = Centre-North, level 3.

discrepancies between the simulated and measured discharge time series. Moreover, differences between LISFLOODFP-HBV and LISFLOODFP-MEAS were larger when using a continuous modeling approach rather than an event-based modeling approach. For instance, in 2012, differences between inundation volumes  $\Delta fv(\alpha, endLHF)$  and extents  $\Delta fe(\alpha, endLHF)$  predicted by LISFLOODFP-HBV and LISFLOODFP-MEAS were  $-3.776 \text{ km}^3$  and  $-3,054$  cells when using a continuous modeling approach ( $\alpha = 1$ ) and  $-1.007 \text{ km}^3$  and  $-1,187$  cells when using an event-based modeling approach ( $\alpha = startLHF$ ).

Results for the Centre-South cluster (level 3) were consistent with the results of the South cluster (level 2) and are not discussed in detail here. No relevant flooding was detected in either LISFLOODFP-HBV or LISFLOODFP-MEAS predictions in the lower area of the MDB, that is, in HRR 26 and 27 (level 4). For this reason, the analysis stopped at level 3 of the hierarchical basin approach.

## 5. Discussion

### 5.1. Study Design and Novelty

The cascading of errors from discharge prediction to floodplain dynamics is highly nonlinear, with previous studies showing that uncertainties and inaccuracies in discharge hydrographs can have a large variability of impacts on the prediction of floodplain inundation dynamics (e.g., McMillan & Brasington, 2008). To add to the current state of knowledge, this paper presented a novel quantitative comparison between input volume discrepancies and floodplain inundation volume discrepancies. A state-of-the-art modeling framework, which was implemented using freely available data sets, was used (a) to provide insight on the challenges, pitfalls, and opportunities for flood inundation modeling at large spatial scales within the current modeling capabilities; and (b) to allow the repeatability of this study in other areas worldwide.

The MDB, Australia's largest river system, was selected as a case study due to its large morphological and climatic variability. The HBV hydrological model was used to simulate discharge hydrographs at 81 locations along the major river network for a 7-year time period (2006–2012). Simulated and measured discharge data were both used to force the hydraulic model LISFLOOD-FP, with the latter model setup used as a benchmark to investigate the impacts of discrepancies in input time series on the prediction of floodplain inundation dynamics. The calibration period and gauge locations for HBV were the same as the modeled period and input points used in LISFLOOD-FP, which was calibrated in a previous study (Schumann et al., 2016).

Rather than engaging in the validation of the predicted floodplain inundation volumes and extents using, for instance, remote sensing observations, the aim of this numerical experiment was to use a state-of-the-art coupled modeling framework to analyze how discrepancies in input time series interact at different

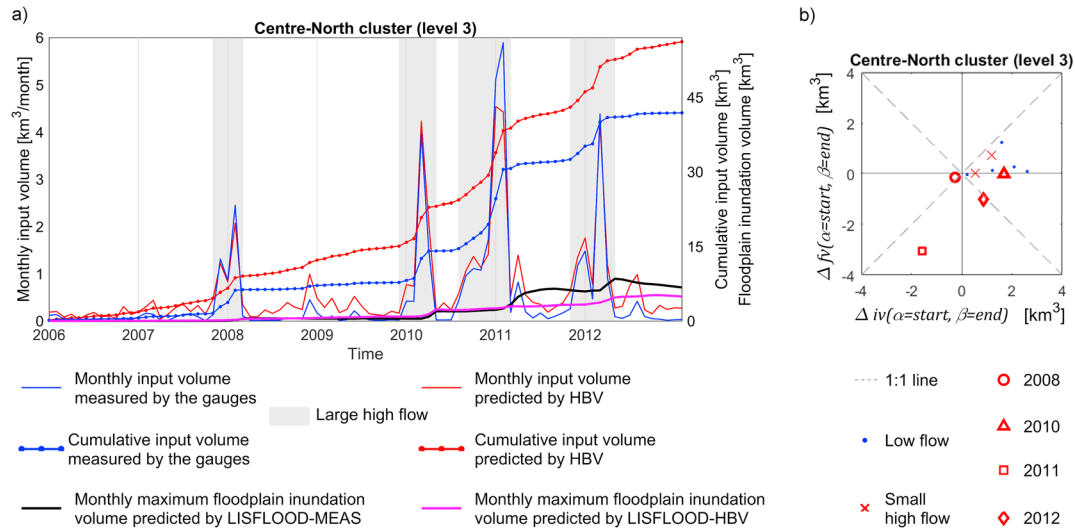


**Figure 5.** Analysis of level 3 cluster: Centre-North cluster. (a) Time series of gauged and modeled input volumes (monthly and cumulative values) and monthly maximum floodplain inundation volumes predicted by LISFLOODFP-MEAS and LISFLOODFP-HBV. (b) Event-based comparison of differences in input volumes and differences in monthly maximum floodplain inundation volumes;  $\Delta iv(\alpha = start, \beta = end)$  and  $\Delta fv(\alpha = start, \beta = end)$  as defined in Table 1, equations 7 and 8, respectively.

temporal and spatial scales via the hydraulic model to produce floodplain inundation patterns. A hierarchical basin approach was used for this purpose and the analysis started with upstream, relatively small, and hydrologically independent subcatchments, which were then progressively aggregated into larger clusters until inclusion of the total basin area. Moreover, differences between results of a continuous modeling approach and an event-based approach were investigated.

### 5.2. Interactions Between Low- and High-Flow Periods at Different Spatial Scales

Understanding the interactions between low- and high-flow periods was essential to explaining floodplain inundation patterns, with upstream, hydrologically independent subcatchments having a strong impact on downstream aggregated clusters. During low-flow periods, simulated input volumes were larger than measured values, but flood wave routing attenuated these discrepancies with the discrepancies in input volumes being larger than the discrepancies in inundation volumes. Such an effect was observed in all the small, upstream subcatchments and all the clusters. During high-flow periods, simulated input volumes were often smaller than measured values. Continuous flood wave routing often partially masked these discrepancies in small, upstream subcatchments, leading to similar inundation volumes for both input time series; this effect was evident in 11 out of 19 subcatchments of level 1. Conversely, when moving from upstream to downstream in large clusters, simulated flood hydrographs smaller than measured ones led to smaller inundation volumes and extents and discrepancies in inundation volumes were higher than discrepancies in input volumes for 7 out of 13 flood events in level 2 and level 3 clusters. In fact, these discrepancies increased during consecutive flood events and, consistently with the analysis of Pappenberger et al. (2005), differences in floodplain inundation volumes triggered by differences in input hydrographs did not fade but rather increased when moving from upstream to downstream. These results demonstrated that discrepancies in input time series are often exacerbated by the hydraulic model for the prediction of floodplain inundation volumes and extents at the large scale. An event-based analysis at different spatial scales was then conducted to investigate factors leading to such an effect.

### 5.3. Higher Relevance of Predictions of Flood Peaks Rather Than Flood Volumes

Analysis of large flow events in upstream subcatchments of level 1 showed that predictions of inundation volume and extent were strongly sensitive to discrepancies in simulated and measured flood peak values. More specifically, in 7 out of 19 subcatchments, values of simulated flood peak lower than measured data resulted in relatively limited overflow from the main river to the floodplain and across the floodplain, thus leading to large floodplain inundation discrepancies. Such a result may help explain the large sensitivity of estimated flood losses to relatively small changes in input hydrographs shown by Sampson et al. (2014) and

Zischg et al. (2018). Moreover, in five large flood events in level 1 subcatchments, measured flood peaks higher than simulated ones led to significantly larger floodplain inundation volumes and extents, despite the simulated input volumes being larger than the measurements. When modeling large clusters, flood peak-driven discrepancies in floodplain inundation dynamics increased with time and in downstream direction, as clearly shown, for instance, in the North-East cluster.

The notion of the relatively large importance of flood peak value compared to flood volumes can guide the development of hydrologic model calibration and error correction strategies. Albeit the use of an objective function that is exclusively based on peak flows is not yet common practice in hydrological modeling at the large scale (Hirpa et al., 2018), implementation of this strategy could leverage on previous experiences at the catchment scale (e.g., Falter et al., 2016; Fenicia et al., 2007; Hostache et al., 2011). However, it is here noted that while this strategy could enhance the predictive performance of the hydrologic model, uncertainties in the simulated streamflow time series and errors in the prediction of the flood peak are likely to persist when precipitation measurements are used as input (e.g., Falter et al., 2016; Hostache et al., 2011) and are expected within a complete flood forecasting chain where precipitation is estimated. Moreover, challenges in the transferability of model parameters calibrated on a historical time series under varying climatic conditions have been demonstrated in a number of studies (Brigode et al., 2013; Romanowicz & Booij, 2015; Vaze et al., 2010). Since uncertainties and errors in hydrograph predictions are (currently) inevitable, this study had the merit to demonstrate the potential magnitude of the impacts of uncertainties in flood peak predictions on floodplain inundation modeling. Enhanced awareness of these uncertainties can support the interpretation of model results; furthermore, investigation of possible joint factors was deemed essential to suggest alternative solutions to improve floodplain inundation prediction skill within the current modeling capabilities.

#### 5.4. Hydrological Regime, Morphological Features, and Simulation Approach

Analysis of inundation dynamics at large temporal and spatial scales showed that the impact of discrepancies between simulated and measured flood peaks was accentuated by a hydrological regime characterized by long dry spells and high-magnitude floods and by peculiar morphological features. Interaction of these effects was evident, for instance, in subcatchment 23 where the impacts of uncertainties in the prediction of flood peaks were exacerbated by a restriction, the Barrackdale Choke, thus leading to discrepancies in inundation volumes and extents that affected inundation predictions in the North-East cluster during all the simulation period. In fact, a lack of adequate representation of critical morphological terrain features in the SRTM DEM likely exacerbated the discrepancies highlighted above. Moreover, as shown, for instance, in the level 3 South cluster, a low accuracy of the floodplain representation can also hinder floodplain drainage in low-slope areas. When modeling a sequence of low- and high-flow periods, underestimation of water withdrawal and the well-known difficulty of accurately predicting low flows (Garcia et al., 2017) can lead to increasing errors in the prediction of floodplain dynamics and can hamper the accurate evaluation of the duration of flooding. Nevertheless, the duration of flooding has a primary role on determining inundation economic and environmental costs (Bates et al., 2018) and the results of this study advocate for more research to improve the modeling skill of the drainage phase of large flood events.

Challenges posed to inundation prediction by the low accuracy of the widely used SRTM DEM (or versions derived thereof) were pointed out in several other analyses (e.g., Bates et al., 2018; Sampson et al., 2015; Sampson et al., 2016; Trigg et al., 2016). To tackle this issue, the creation of a new open-access high-accuracy global DEM is being strongly advocated for by the flooding community (e.g., Sampson et al., 2016; Schumann et al., 2014). Moreover, error-corrected versions of the SRTM DEM such as the Australian 1-arc-sec-resolution Hydrologically Enforced DEM (Gallant, Read, & Dowling, 2011; Gallant, Wilson, et al., 2011) and the global 3-arc-sec-resolution “Multi-Error-Removed Improved-Terrain DEM (MERIT DEM)” (Yamazaki et al., 2017) have been released, and strategies to enhance the efficiency of DEMs for hydraulic modeling have been proposed (e.g., Baugh et al., 2013; Chen et al., 2018; Hirt, 2018; Jarihani et al., 2015; Mason et al., 2016; O’Loughlin et al., 2016). However, any DEM is inherently affected by errors and uncertainties, especially in highly complex morphological areas. For instance, Falter et al. (2016) showed that inaccurate representation of morphological features led to large errors in the prediction of floodplain extents despite the fact that the terrain representation was based on a 10-m resolution with  $\pm 0.5$ - to 2-m vertical accuracy database. Consequently, the methodology presented in this study, albeit

simple and based on the modeling of two time series only, could be used to identify areas requiring more accurate terrain representation and provide advice for targeted data collections.

Finally, the quantitative comparison developed in this study, showed that floodplain inundation uncertainties and cascading errors due to the hydrological regime, morphological peculiarities, and the low accuracy of digital terrain models all accumulated in a continuous modeling approach. Conversely, discrepancies could be reduced by using an event-based approach. Based on this insight, assimilation of inundation extents and/or water level in both low- and high-flow periods may provide a pragmatic strategy to achieve acceptable skill in time-continuous flood modeling; however, testing of a data assimilation strategy is out of scope of this paper.

### 5.5. Significance of the Study, Limitations, and Future Work

This study focused on one source of uncertainty (i.e., discrepancies between simulated and measured flood hydrograph features) with the aim of providing a better understanding of the relationships between discharge, flow paths, and inundation volumes as well as flood extents. In fact, a prediction scenario should contemplate ensemble flood forecasting (Cloke & Pappenberger, 2009) and a thorough evaluation of all the sources of uncertainty in order to produce probabilistic maps of inundation extents and levels. However, computational constraints still limit the number of model runs that can be made in both an offline and real-time forecasting scenario (Bates et al., 2018). In this context, it is worth noting that the simple approach of this study, in which only two flow time series were routed through a hydraulic model, was capable of pinpointing areas critical for improving flood inundation modeling. For instance, the particular flooding behavior of the Paroo and Warrego Rivers in HRR 24 and 25 (North-West area of the MDB) due to the complexity of the river and floodplain network was highlighted. A conceptual validation of this result was found in previous studies based on the analysis of field and remote sensing (Landsat) data. In fact, Bunn et al. (2006) and Heimhuber et al. (2016, 2017) showed that frequent and relatively low flow pulses in the Paroo region lead to in-channel flows without achieving floodplain inundation; conversely, increasing river discharge values lead to a saturation point of incipient flooding, above which rare high peak flows cause a large increase in surface water extent.

This study highlighted the importance of an accurate prediction of flood peak values for floodplain inundation modeling. Moreover, event-based modeling and data assimilation in low and dry periods were envisaged as pragmatic solutions to improve floodplain inundation forecast skill. Conceptualization of the outcomes of this study can be readily applied to improve the accuracy of long-term flow modeling in the MDB, thus providing a powerful tool to (i) support flood forecast and risk analysis (e.g., Domeneghetti et al., 2018), (ii) complement remote sensing-based investigations of surface flow connectivity and its ecological implications (e.g., Bishop-Taylor et al., 2015; Bishop-Taylor et al., 2018; Heimhuber et al., 2016, 2017; Huang et al., 2014; Tulbure et al., 2016), and (iii) support investigation of groundwater recharge due to flooding (e.g., Doble et al., 2014).

Clearly, care should be taken when extrapolating the results of this numerical experiment to other basins, with different morphologic characteristics and climatic conditions. In fact, as Bates et al. (2018) recently stated, output from large-scale models should be treated differently across different climate zones. However, it should be noted that similarly to the MDB, many other large catchments worldwide have a complex river network and experience large interannual and interdecadal hydrological variability associated with climate modes such as El Niño-Southern Oscillation, Pacific Decadal Oscillation, and the North Atlantic Oscillation. Moreover, current climate change projection studies highlight a possible amplification of wet and dry extremes (e.g., Armal et al., 2018; Betts et al., 2018; Lu et al., 2018; Taye et al., 2015; Trenberth et al., 2003). Furthermore, the large impact of local morphologic features highlighted in this study alludes to the importance of accounting for the potential impact of flood defenses in flood inundation prediction models, although a complete and accessible database of such infrastructure is currently not available, except for a very limited number of countries or regions. In fact, it is suggested that the presented methodology can be applied to other basins in order to define areas requiring tailored modeling solutions, plan for resources and investments for data collection (e.g., survey of river banks, natural restrictions, and levee systems), and support the understanding of the main drivers of uncertainty within a modeling cascade.

### Acknowledgments

Stefania Grimaldi is funded through the Bushfire and Natural Hazards Collaborative Research Centre grant "Improving Flood Forecast Skill Using Remote Sensing Data." Ashkan Shokri acknowledges the support from Monash University in the form of a Monash Graduate Scholarship (MGS) and Monash International Postgraduate Research Scholarship (MIPRS). The authors thank Francesco Dottori, the two anonymous reviewers, the Associate Editor, and the Editor who provided comments that helped improve the quality of the manuscript. Tables S1–S3 are available in the supporting information. Measured 0.01° maps of daily precipitation data were provided by the Australian Bureau of Meteorology (<http://www.bom.gov.au/climate/austmaps/metadata-daily-rainfall.shtml>) and can be obtained from the Australian National University Climate database, available from the data catalog hosted by the Australian National Computational Infrastructure (<http://dapds00.nci.org.au/thredds/catalog/ub8/au/climate/catalog.html>). Monthly 0.01° maps of potential evapotranspiration data were generated using the eMAST R package, hosted by the Australian National Computational Infrastructure ([http://dapds00.nci.org.au/thredds/catalog/rr9/eMAST-R-Package/eMAST-R-Package\\_v1-1\\_potential-evapotranspiration\\_monthly\\_0-01deg\\_1970-2012/00000000/catalog.html](http://dapds00.nci.org.au/thredds/catalog/rr9/eMAST-R-Package/eMAST-R-Package_v1-1_potential-evapotranspiration_monthly_0-01deg_1970-2012/00000000/catalog.html)). Satellite-derived GLEAM (Global Land Evaporation Amsterdam Model) evapotranspiration losses can be downloaded from <https://www.gleam.eu/>. Hourly time series of discharge observations are available from New South Wales Office of Water ([http://realtime-data.water.nsw.gov.au/water.stm?ppbm=DAILY\\_REPORTS&dr&3&drkd\\_url](http://realtime-data.water.nsw.gov.au/water.stm?ppbm=DAILY_REPORTS&dr&3&drkd_url)), Queensland Department of Natural Resources and Mines (<http://watermonitoring.derm.qld.gov.au/host.htm>), and Victoria Department of Environment and Primary Industries (<http://www.vicwaterdata.net/vicwaterdata/home.aspx>). The Australian Hydrological Geospatial Fabric (Geofabric) including the Hydrology Reporting Regions and the river network is available from the Australian Bureau of Meteorology (<http://www.bom.gov.au/water/geofabric/index.shtml>). The SRTM digital elevation model is available from <https://www2.jpl.nasa.gov/srtm/>. LISFLOODFP is available for noncommercial research purposes by contacting Paul Bates at the University of Bristol ([paul.bates@bristol.ac.uk](mailto:paul.bates@bristol.ac.uk)).

## 6. Conclusions

Accurate predictions of spatiotemporal patterns of flooding as well as surface water dynamics are essential to reduce flood-related damage, increase resilience, improve flood risk estimation, allow equitable management of global resources, and improve ecological systems services (e.g., Falter et al., 2015; Hanjra & Qureshi, 2010; Ward et al., 2015). Coupled hydrologic-hydraulic models are at the core of flood forecasting and risk assessment models. In simple words, hydrologic models are used to predict discharge hydrographs, which are then used as input to hydraulic models for the prediction of floodplain inundation dynamics. This study used a numerical experiment to investigate the effects of discrepancies between simulated and measured discharge hydrographs on the prediction of floodplain inundation volumes and extents. Although based on a specific large-scale case study, the presented methodology can be applied to other basins in order to define areas requiring tailored modeling solutions and suggest resource investments for data collection.

Complex morphological features and low-accuracy topographic data hamper accurate flood modeling at the basin scale, with inundation prediction uncertainties during low-flow periods strongly affecting modeling results across high-flow periods. The analysis presented here highlights the large sensitivity of floodplain dynamics to peak discharge values and the limitations of a time-continuous flood modeling approach under such conditions. Consequently, it is suggested that more accurate peak discharge predictions, better knowledge about critical morphologic terrain features, and data assimilation of inundation extents and water levels in both low- and high-flow periods may provide a pragmatic strategy to achieve acceptable skill in time-continuous flood inundation modeling.

These conclusions can help improve forecast skill within the current modeling and implementation capabilities, proactively contribute to recent efforts in the definition of more comprehensive methodologies for the evaluation of flow forecasts (e.g., Cloke et al., 2017; Wetterhall et al., 2013), provide valuable guidance for modeling choices, and support communication of uncertainties in model results to end users.

## References

- Alfieri, L., Burek, P., Dutra, E., Krzeminski, B., Muraro, D., Thielen, J., & Pappenberger, F. (2013). GloFAS—Global ensemble streamflow forecasting and flood early warning. *Hydrology and Earth System Sciences*, *17*(3), 1161–1175. <https://doi.org/10.5194/hess-17-1161-2013>
- Alfieri, L., Cohen, S., Galantowicz, J., Schumann, G. J. P., Trigg, M. A., Zsoter, E., et al. (2018). A global network for operational flood risk reduction. *Environmental Science & Policy*, *84*, 149–158. <https://doi.org/10.1016/j.envsci.2018.03.014>
- Alfieri, L., Salamon, P., Bianchi, A., Neal, J., Bates, P., & Feyen, L. (2014). Advances in pan-European flood hazard mapping. *Hydrological Processes*, *28*(13), 4067–4077. <https://doi.org/10.1002/hyp.9947>
- Andreadis, K. M., Schumann, G. J. P., & Pavelsky, T. (2013). A simple global river bankfull width and depth database. *Water Resources Research*, *49*, 7164–7168. <https://doi.org/10.1002/wrcr.20440>
- Armal, S., Devineni, N., & Khanbilvardi, R. (2018). Trends in extreme rainfall frequency in the Contiguous United States: Attribution to climate change and climate variability modes. *Journal of Climate*, *31*(1), 369–385. <https://doi.org/10.1175/jcli-d-17-0106.1>
- Arthington, A. H., & Balcombe, S. R. (2011). Extreme flow variability and the 'boom and bust' ecology of fish in arid-zone floodplain rivers: A case history with implications for environmental flows, conservation and management. *Ecohydrology*, *4*(5), 708–720. <https://doi.org/10.1002/eco.221>
- Australian Bureau of Meteorology. (2015). Australian Hydrological Geospatial Fabric (Geofabric) product guide. Retrieved from <http://www.bom.gov.au/water/geofabric/index.shtml>
- Bates, P. D., Horritt, M. S., & Fewtrell, T. J. (2010). A simple inertial formulation of the shallow water equations for efficient two-dimensional flood inundation modelling. *Journal of Hydrology*, *387*(1–2), 33–45. <https://doi.org/10.1016/j.jhydrol.2010.03.027>
- Bates, P. D., Neal, J., Sampson, C., Smith, A., & Trigg, M. (2018). Chapter 9—Progress toward hyperresolution models of global flood hazard. In *Risk modeling for hazards and disasters* (pp. 211–232). Oxford, UK: Elsevier.
- Baugh, C. A., Bates, P. D., Schumann, G., & Trigg, M. A. (2013). SRTM vegetation removal and hydrodynamic modeling accuracy. *Water Resources Research*, *49*, 5276–5289. <https://doi.org/10.1002/wrcr.20412>
- Betts, R. A., Alfieri, L., Bradshaw, C., Caesar, J., Feyen, L., Friedlingstein, P., et al. (2018). Changes in climate extremes, fresh water availability and vulnerability to food insecurity projected at 1.5°C and 2°C global warming with a higher-resolution global climate model. *Philosophical Transactions of the Royal Society A: Mathematical, Physical and Engineering Sciences*, *376*(2119). <https://doi.org/10.1098/rsta.2016.0452>
- Biancamaria, S., Bates, P. D., Boone, A., & Mognard, N. M. (2009). Large-scale coupled hydrologic and hydraulic modelling of the Ob river in Siberia. *Journal of Hydrology*, *379*(1–2), 136–150. <https://doi.org/10.1016/j.jhydrol.2009.09.054>
- Bishop-Taylor, R., Tulbure, M., & Broich, M. (2015). Surface water network structure, landscape resistance to movement and flooding vital for maintaining ecological connectivity across Australia's largest river basin. *Landscape Ecology*, *30*(10), 2045–2065. <https://doi.org/10.1007/s10980-015-0230-4>
- Bishop-Taylor, R., Tulbure, M. G., & Broich, M. (2018). Evaluating static and dynamic landscape connectivity modelling using a 25-year remote sensing time series. *Landscape Ecology*, *33*(4), 625–640. <https://doi.org/10.1007/s10980-018-0624-1>
- Bonnifant, L., Delrieu, G., Le Lay, M., Boudevillain, B., Masson, A., Belleudy, P., et al. (2009). Distributed hydrologic and hydraulic modelling with radar rainfall input: Reconstruction of the 8–9 September 2002 catastrophic flood event in the Gard region, France. *Advances in Water Resources*, *32*, 1077–1089. <https://doi.org/10.1016/j.advwatres.2009.03.007>

- Bravo, J. M., Allasia, D., Paz, A. R., Collischon, W., & Tucci, C. E. M. (2012). Coupled hydrologic-hydraulic modeling of the Upper Paraguay River Basin. *Journal of Hydrologic Engineering*, *17*(5), 635–646. [https://doi.org/10.1061/\(ASCE\)HE.1943-5584.0000494](https://doi.org/10.1061/(ASCE)HE.1943-5584.0000494)
- Brigode, P., Oudin, L., & Perrin, C. (2013). Hydrological model parameter instability: A source of additional uncertainty in estimating the hydrological impacts of climate change? *Journal of Hydrology*, *476*, 410–425. <https://doi.org/10.1016/j.jhydrol.2012.11.012>
- Bunn, S. E., Thoms, M. C., Hamilton, S. K., & Capon, S. J. (2006). Flow variability in dryland rivers: Boom, bust and the bits in between. *River Research and Applications*, *22*(2), 179–186. <https://doi.org/10.1002/rra.904>
- Chen, H., Liang, Q., Liu, Y., & Xie, S. (2018). Hydraulic correction method (HCM) to enhance the efficiency of SRTM DEM in flood modeling. *Journal of Hydrology*, *559*, 56–70. <https://doi.org/10.1016/j.jhydrol.2018.01.056>
- Cloke, H., & Pappenberger, F. (2009). Ensemble flood forecasting: A review. *Journal of Hydrology*, *375*(3–4), 613–626. <https://doi.org/10.1016/j.jhydrol.2009.06.005>
- Cloke, H. L., Pappenberger, F., Smith, P. J., & Wetterhall, F. (2017). How do I know if I've improved my continental scale flood early warning system? *Environmental Research Letters*, *12*(4), 044006. <https://doi.org/10.1088/1748-9326/aa625a>
- Doble, R., Crosbie, R., Peeters, L., Joehnk, K., & Ticehurst, C. (2014). Modelling overbank flood recharge at a continental scale. *Hydrology and Earth System Sciences*, *18*, 1273–1288. <https://doi.org/10.5194/hess-18-1273-2014>
- Domeneghetti, A. (2016). On the use of SRTM and altimetry data for flood modeling in data-sparse regions. *Water Resources Research*, *52*, 2901–2918. <https://doi.org/10.1002/2015WR017967>
- Domeneghetti, A., Ceola, S., Colanzi, P., & Schumann, G. (2018). Evaluation of flood risk evolution on the Murray-Darling Basin (Australia) from 1975 to 2014 combining a hydrodynamic model and remote sensing data. Paper presented at the EGU General Assembly 2018, Vienna (Austria), <https://doi.org/10.1155/2018/6148351>
- Domingo, N. D. S., Refsgaard, A., Mark, O., & Paludan, B. (2010). Flood analysis in mixed-urban areas reflecting interactions with the complete water cycle through coupled hydrologic-hydraulic modelling. *Water Science and Technology*, *62*(6), 1386–1392. <https://doi.org/10.2166/wst.2010.365>
- Dottori, F., Salamon, P., Bianchi, A., Alfieri, L., Hirpa, F. A., & Feyen, L. (2016). Development and evaluation of a framework for global flood hazard mapping. *Advances in Water Resources*, *94*, 87–102. <https://doi.org/10.1016/j.advwatres.2016.05.002>
- Dottori, F., Szewczyk, W., Ciscar, J.-C., Zhao, F., Alfieri, L., Hirabayashi, Y., et al. (2018). Increased human and economic losses from river flooding with anthropogenic warming. *Nature Climate Change*, *8*(9), 781–786. <https://doi.org/10.1038/s41558-018-0257-z>
- Emerton, R. E., Stephens, E. M., Pappenberger, F., Pagano, T. C., Weerts, A. H., Wood, A. W., et al. (2016). Continental and global scale flood forecasting systems. *Wiley Interdisciplinary Reviews: Water*, *3*(3), 391–418. <https://doi.org/10.1002/wat2.1137>
- Falter, D., Dung, N. V., Vorogushyn, S., Schröter, K., Hundedcha, Y., Kreibich, H., et al. (2016). Continuous, large-scale simulation model for flood risk assessments: Proof-of-concept. *Journal of Flood Risk Management*, *9*(1), 3–21. <https://doi.org/10.1111/jfr3.12105>
- Falter, D., Schröter, K., Dung, N. V., Vorogushyn, S., Kreibich, H., Hundedcha, Y., et al. (2015). Spatially coherent flood risk assessment based on long-term continuous simulation with a coupled model chain. *Journal of Hydrology*, *524*, 182–193. <https://doi.org/10.1016/j.jhydrol.2015.02.021>
- Felder, G., Zischg, A., & Weingartner, R. (2017). The effect of coupling hydrologic and hydrodynamic models on probable maximum flood estimation. *Journal of Hydrology*, *550*, 157–165. <https://doi.org/10.1016/j.jhydrol.2017.04.052>
- Fenicia, F., Solomatine, D., Savenije, H., & Matgen, P. (2007). Soft combination of local models in a multi-objective framework. *Hydrology and Earth System Sciences Discussions*, *11*(6), 1797–1809. <https://doi.org/10.5194/hess-11-1797-2007>
- Gallant, J., Read, A., & Dowling, T. (2011). Building a high resolution national elevation model from SRTM: The Australian experience. Paper presented at the AGU Fall Meeting Abstracts.
- Gallant, J. C., Wilson, N., Dowling, T. I., Read, A., & Inskip, C. (2011). 1 second SRTM derived products user guide Retrieved from [https://d28rz98at9flks.cloudfront.net/72759/1secSRTM\\_Derived\\_DEMs\\_UserGuide\\_v1.0.4.pdf](https://d28rz98at9flks.cloudfront.net/72759/1secSRTM_Derived_DEMs_UserGuide_v1.0.4.pdf), <https://doi.org/10.1093/cid/cir689>
- García, F., Folton, N., & Oudin, L. (2017). Which objective function to calibrate rainfall-runoff models for low-flow index simulations? *Hydrological Sciences Journal*, *62*(7), 1149–1166. <https://doi.org/10.1080/02626667.2017.1308511>
- Giustarini, L., Matgen, P., Hostache, R., Montanari, M., Plaza, D., Pauwels, V. R. N., et al. (2011). Assimilating SAR-derived water level data into a hydraulic model: A case study. *Hydrology and Earth System Sciences Discussions*, *8*(1), 2103–2144. <https://doi.org/10.5194/hessd-8-2103-2011>
- Grimaldi, S., Petroselli, A., Arcangeletti, E., & Nardi, F. (2013). Flood mapping in ungauged basins using fully continuous hydrologic-hydraulic modeling. *Journal of Hydrology*, *487*, 39–47. <https://doi.org/10.1016/j.jhydrol.2013.02.023>
- Gül, G. O., Harmancıoğlu, N., & Gül, A. (2010). A combined hydrologic and hydraulic modeling approach for testing efficiency of structural flood control measures. *Natural Hazards*, *54*(2), 245–260. <https://doi.org/10.1007/s11069-009-9464-2>
- Hanjra, M. A., & Qureshi, M. E. (2010). Global water crisis and future food security in an era of climate change. *Food Policy*, *35*(5), 365–377. <https://doi.org/10.1016/j.foodpol.2010.05.006>
- Heimhuber, V., Tulbure, M. G., & Broich, M. (2016). Modeling 25 years of spatio-temporal surface water and inundation dynamics on large river basin scale using time series of Earth observation data. *Hydrology and Earth System Sciences*, *20*(6), 2227–2250. <https://doi.org/10.5194/hess-20-2227-2016>
- Heimhuber, V., Tulbure, M. G., & Broich, M. (2017). Modeling multidecadal surface water inundation dynamics and key drivers on large river basin scale using multiple time series of Earth—Observation and river flow data. *Water Resources Research*, *53*, 1251–1269. <https://doi.org/10.1002/2016WR019858>
- Hirabayashi, Y., Mahendran, R., Koirala, S., Konoshima, L., Yamazaki, D., Watanabe, S., et al. (2013). Global flood risk under climate change. *Nature Climate Change*, *3*(9), 816–821. <https://doi.org/10.1038/nclimate1911>, <https://www.nature.com/articles/nclimate1911#supplementary-information>
- Hirpa, F. A., Salamon, P., Beck, H. E., Lorini, V., Alfieri, L., Zsoter, E., & Dadson, S. J. (2018). Calibration of the Global Flood Awareness System (GloFAS) using daily streamflow data. *Journal of Hydrology*, *566*, 595–606. <https://doi.org/10.1016/j.jhydrol.2018.09.052>
- Hirt, C. (2018). Artefact detection in global digital elevation models (DEMs): The maximum slope approach and its application for complete screening of the SRTM v4.1 and MERIT DEMs. *Remote Sensing of Environment*, *207*, 27–41. <https://doi.org/10.1016/j.rse.2017.12.037>
- Hostache, R., Matgen, P., Montanari, A., Montanari, M., Hoffmann, L., & Pfister, L. (2011). Propagation of uncertainties in coupled hydro-meteorological forecasting systems: A stochastic approach for the assessment of the total predictive uncertainty. *Atmospheric Research*, *100*(2–3), 263–274. <https://doi.org/10.1016/j.atmosres.2010.09.014>
- Huang, C., Chen, Y., & Wu, J. (2013). GIS-based spatial zoning for flood inundation modelling in the Murray-Darling Basin. Paper presented at the 20th International Congress on Modelling and Simulation, Adelaide (Australia).

- Huang, C., Chen, Y., & Wu, J. (2014). Mapping spatio-temporal flood inundation dynamics at large river basin scale using time-series flow data and MODIS imagery. *International Journal of Applied Earth Observation and Geoinformation*, *26*, 350–362. <https://doi.org/10.1016/j.jag.2013.09.002>
- Huang, S., & Hattermann, F. F. (2018). Coupling a global hydrodynamic algorithm and a regional hydrological model for large-scale flood inundation simulations. *Hydrology Research*, *49*(2), 438–449. <https://doi.org/10.2166/nh.2017.061>
- Jarihani, A. A., Callow, J. N., McVicar, T. R., Van Niel, T. G., & Larsen, J. R. (2015). Satellite-derived digital elevation model (DEM) selection, preparation and correction for hydrodynamic modelling in large, low-gradient and data-sparse catchments. *Journal of Hydrology*, *524*, 489–506. <https://doi.org/10.1016/j.jhydrol.2015.02.049>
- Jones, D. A., Wang, W., & Fawcett, R. (2009). High-quality spatial climate data-sets for Australia. *Australian Meteorological and Oceanographic Journal*, *58*(04), 233–248. <https://doi.org/10.22499/2.5804.003>
- Kennedy, J., & Eberhart, R. (1995). Particle swarm Optimization. Paper presented at the International Conference on Neural Networks, Piscataway, N.J.
- Kleynhans, M. T., James, C. S., & Birkhead, A. L. (2007). Hydrologic and hydraulic modelling of the Nyl River floodplain Part 3: Applications to assess ecological impact. *Water SA*, *33*(1), 21–25. <https://doi.org/10.4314/wsa.v33i1.47867>
- Komi, K., Neal, J., Trigg, M. A., & Diekkrüger, B. (2017). Modelling of flood hazard extent in data sparse areas: A case study of the Oti River basin, West Africa. *Journal of Hydrology: Regional Studies*, *10*, 122–132. <https://doi.org/10.1016/j.ejrh.2017.03.001>
- Laganier, O., Ayrat, P. A., Salze, D., & Sauvagnargues, S. (2014). A coupling of hydrologic and hydraulic models appropriate for the fast floods of the Gardon river basin (France): Results and comparisons with others modelling options. *Natural Hazards and Earth System Sciences*, *14*(11), 2899–2920. <https://doi.org/10.5194/nhess-14-2899-2014>
- Leblanc, M., Tweed, S., Van Dijk, A., & Timbal, B. (2012). A review of historic and future hydrological changes in the Murray-Darling Basin. *Global and Planetary Change*, *80*, 226–246.
- Lehner, B., & Döll, P. (2004). Development and validation of a global database of lakes, reservoirs and wetlands. *Journal of Hydrology*, *296*(1–4), 1–22. <https://doi.org/10.1016/j.jhydrol.2004.03.028>
- Lerat, J. (2009). Quels apports hydrologiques pour les modèles hydrauliques? Vers un modèle intégré de simulation des crues. Université Pierre et Marie Curie-Paris VI.
- Lian, Y., Chan, I.-C., Singh, J., Demissie, M., Knapp, V., & Xie, H. (2007). Coupling of hydrologic and hydraulic models for the Illinois River Basin. *Journal of Hydrology*, *344*(3–4), 210–222. <https://doi.org/10.1016/j.jhydrol.2007.08.004>
- Lindström, G., Johansson, B., Persson, M., Gardelin, M., & Bergström, S. (1997). Development and test of the distributed HBV-96 hydrological model. *Journal of Hydrology*, *201*(1–4), 272–288. [https://doi.org/10.1016/S0022-1694\(97\)00041-3](https://doi.org/10.1016/S0022-1694(97)00041-3)
- Lu, J., Xue, D., Gao, Y., Chen, G., Leung, L. R., & Staten, P. (2018). Enhanced hydrological extremes in the western United States under global warming through the lens of water vapor wave activity. *Climate and Atmospheric Science*, *1*(1). <https://doi.org/10.1038/s41612-018-0017-9>
- Mai, D., & De Smedt, F. (2017). A combined hydrological and hydraulic model for flood prediction in Vietnam applied to the Huong River basin as a test case study. *Water*, *9*(11), 879. <https://doi.org/10.3390/w9110879>
- Martens, B., Miralles, D. G., Lievens, H., van der Schalie, R., de Jeu, R. A., Fernández-Prieto, D., et al. (2017). GLEAM v3: Satellite-based land evaporation and root-zone soil moisture. *Geoscientific Model Development*, *10*(5), 1903–1925. <https://doi.org/10.5194/gmd-10-1903-2017>
- Mason, D. C., Trigg, M., Garcia-Pintado, J., Cloke, H. L., Neal, J. C., & Bates, P. D. (2016). Improving the TanDEM-X digital elevation model for flood modelling using flood extents from synthetic aperture radar images. *Remote Sensing of Environment*, *173*, 15–28. <https://doi.org/10.1016/j.rse.2015.11.018>
- Matgen, P., Montanari, M., Hostache, R., Pfister, L., Hoffmann, L., Plaza, D., et al. (2010). Towards the sequential assimilation of SAR-derived water stages into hydraulic models using the Particle Filter: Proof of concept. *Hydrology and Earth System Sciences*, *14*(9), 1773–1785. <https://doi.org/10.5194/hess-14-1773-2010>
- McMillan, H. K., & Brasington, J. (2008). End-to-end flood risk assessment: A coupled model cascade with uncertainty estimation. *Water Resources Research*, *44*, W03419. <https://doi.org/10.1029/2007WR005995>
- Mejia, A., & Reed, S. (2011). Evaluating the effects of parameterized cross section shapes and simplified routing with a coupled distributed hydrologic and hydraulic model. *Journal of Hydrology*, *409*(1–2), 512–524. <https://doi.org/10.1016/j.jhydrol.2011.08.050>
- Miralles, D., Holmes, T., De Jeu, R., Gash, J., Meesters, A., & Dolman, A. (2011). Global land-surface evaporation estimated from satellite-based observations. *Hydrology and Earth System Sciences*, *15*(2), 453–469. <https://doi.org/10.5194/hess-15-453-2011>
- Montanari, M., Hostache, R., Matgen, P., Schumann, G., Pfister, L., & Hoffmann, L. (2009). Calibration and sequential updating of a coupled hydrologic-hydraulic model using remote sensing-derived water stages. *Hydrology and Earth System Sciences*, *13*(3), 367–380. <https://doi.org/10.5194/hess-13-367-2009>
- Moretti, G., & Orlandini, S. (2017). Hydrography-driven coarsening of grid digital elevation models. *Water Resources Research*, *54*, 3654–3672. <https://doi.org/10.1029/2017WR021206>
- Mueller, N., Lewis, A., Roberts, D., Ring, S., Melrose, R., Sixsmith, J., et al. (2016). Water observations from space: Mapping surface water from 25 years of Landsat imagery across Australia. *Remote Sensing of Environment*, *174*, 341–352. <https://doi.org/10.1016/j.rse.2015.11.003>
- Murray-Darling Basin Authority. (2010). Guide to the proposed Basin Plan: Technical background. Canberra (AUS).
- Nam, D. H., Mai, D. T., Udo, K., & Mano, A. (2014). Short-term flood inundation prediction using hydrologic-hydraulic models forced with downscaled rainfall from global NWP. *Hydrological Processes*, *28*(24), 5844–5859. <https://doi.org/10.1002/hyp.10084>
- Nania, L. S., León, A. S., & García, M. H. (2014). Hydrologic-hydraulic model for simulating dual drainage and flooding in urban areas: application to a catchment in the metropolitan area of Chicago. *Journal of Hydrologic Engineering*, *20*(5). [https://doi.org/10.1061/\(ASCE\)HE.1943-5584.0001080](https://doi.org/10.1061/(ASCE)HE.1943-5584.0001080)
- Nash, J. E., & Sutcliffe, J. V. (1970). River flow forecasting through conceptual models part I—A discussion of principles. *Journal of Hydrology*, *10*(3), 282–290. [https://doi.org/10.1016/0022-1694\(70\)90255-6](https://doi.org/10.1016/0022-1694(70)90255-6)
- Neal, J., Dunne, T., Sampson, C., Smith, A., & Bates, P. (2018). Optimisation of the two-dimensional hydraulic model LISFOOD-FP for CPU architecture. *Environmental Modelling & Software*, *107*, 148–157. <https://doi.org/10.1016/j.envsoft.2018.05.011>
- Neal, J., Keef, C., Bates, P., Beven, K., & Leedal, D. (2013). Probabilistic flood risk mapping including spatial dependence. *Hydrological Processes*, *27*(9), 1349–1363. <https://doi.org/10.1002/hyp.9572>
- Neal, J., Schumann, G., & Bates, P. (2012). A subgrid channel model for simulating river hydraulics and floodplain inundation over large and data sparse areas. *Water Resources Research*, *48*, W11506. <https://doi.org/10.1029/2012WR012514>

- Neal, J., Villanueva, I., Wright, N., Willis, T., Fewtrell, T., & Bates, P. (2012). How much physical complexity is needed to model flood inundation? *Hydrological Processes*, *26*(15), 2264–2282. <https://doi.org/10.1002/hyp.8339>
- Nguyen, P., Thorstensen, A., Sorooshian, S., Hsu, K., AghaKouchak, A., Sanders, B., et al. (2016). A high resolution coupled hydrologic-hydraulic model (HiResFlood-UCI) for flash flood modeling. *Journal of Hydrology*, *541*, Part A, 401–420. <https://doi.org/10.1016/j.jhydrol.2015.10.047>
- O'Loughlin, F. E., Paiva, R. C. D., Durand, M., Alsdorf, D. E., & Bates, P. D. (2016). A multi-sensor approach towards a global vegetation corrected SRTM DEM product. *Remote Sensing of Environment*, *182*, 49–59. <https://doi.org/10.1016/j.rse.2016.04.018>
- Pappenberger, F., Beven, K., Hunter, M., Bates, P. D., Gouweleeuw, T., Thielen, J., & Roo, A. (2005). Cascading model uncertainty from medium range weather forecasts (10 days) through a rainfall-runoff model to flood inundation predictions within the European Flood Forecasting System (EFFS). *Hydrology and Earth System Sciences*, *9*(4), 381–393. <https://doi.org/10.5194/hess-9-381-2005>
- Pauwels, V. R. N., De Lannoy, G. J. M., Hendricks Franssen, H.-J., & Vereecken, H. (2013). Simultaneous estimation of model state variables and observation and forecast biases using a two-stage hybrid Kalman filter. *Hydrology and Earth System Sciences Discussions*, *10*(4), 5169–5224. <https://doi.org/10.5194/hessd-10-5169-2013>
- Penton, D., & Overton, I. (2007). Spatial modelling of floodplain inundation combining satellite imagery and elevation models. Paper presented at the MODSIM 2007 International Congress on Modelling and Simulation, Modelling and Simulation Society of Australia and New Zealand CSIRO, Clayton south, Vic, Australia.
- Rodríguez-Rincón, J., Pedrozo-Acuña, A., & Breña-Naranjo, J. (2015). Propagation of hydro-meteorological uncertainty in a model cascade framework to inundation prediction. *Hydrology and Earth System Sciences*, *19*(7), 2981–2998. <https://doi.org/10.5194/hess-19-2981-2015>
- Romanowicz, R. J., & Booij, M. J. (2015). The influence of parametric uncertainty on the relationships between HBV model parameters and climatic characteristics AU - Osuch, Marzena. *Hydrological Sciences Journal*, *60*(7-8), 1299–1316. <https://doi.org/10.1080/02626667.2014.967694>
- Sampson, C. C., Fewtrell, T. J., O'Loughlin, F., Pappenberger, F., Bates, P. B., Freer, J. E., & Cloke, H. L. (2014). The impact of uncertain precipitation data on insurance loss estimates using a flood catastrophe model. *Hydrology and Earth System Sciences*, *18*(6), 2305–2324. <https://doi.org/10.5194/hess-18-2305-2014>
- Sampson, C. C., Smith, A. M., Bates, P. D., Neal, J. C., Alfieri, L., & Freer, J. E. (2015). A high-resolution global flood hazard model. *Water Resources Research*, *51*, 7358–7381. <https://doi.org/10.1002/2015WR016954>
- Sampson, C. C., Smith, A. M., Bates, P. D., Neal, J. C., & Trigg, M. A. (2016). Perspectives on open access high resolution digital elevation models to produce global flood hazard layers. *Frontiers in Earth Science*, *3*(85), 3. <https://doi.org/10.3389/feart.2015.00085>
- Schumann, G., D Bates, P., Neal, J., & Andreadis, K. (2014). Technology: Fight floods on a global scale. *Nature*, *507*(7491), 169. <https://doi.org/10.1038/507169e>
- Schumann, G. J. P., Neal, J. C., Voisin, N., Andreadis, K. M., Pappenberger, F., Phanhuwongpakdee, N., et al. (2013). A first large-scale flood inundation forecasting model. *Water Resources Research*, *49*, 6248–6257. <https://doi.org/10.1002/wrcr.20521>
- Schumann, G. J. P., Stampoulis, D., Smith, A. M., Sampson, C. C., Andreadis, K. M., Neal, J. C., & Bates, P. D. (2016). Rethinking flood hazard at the global scale. *Geophysical Research Letters*, *43*, 10,249–210,256. <https://doi.org/10.1002/2016GL070260>
- Simard, M., Pinto, N., Fisher, J. B., & Baccini, A. (2011). Mapping forest canopy height globally with spaceborne lidar. *Journal of Geophysical Research*, *116*, G04021. <https://doi.org/10.1029/2011JG001708>
- Sindhu, K., & Durga, R. K. H. V. (2017). Hydrological and hydrodynamic modeling for flood damage mitigation in Brahmani-Baitarani River Basin, India. *Geocarto International*, *32*(9), 1004–1016. <https://doi.org/10.1080/10106049.2016.1178818>
- Taye, M. T., Willems, P., & Block, P. (2015). Implications of climate change on hydrological extremes in the Blue Nile basin: A review. *Journal of Hydrology: Regional Studies*, *4*, 280–293. <https://doi.org/10.1016/j.ejrh.2015.07.001>
- Thielen-del Pozo, J., Thiemi, V., Pappenberger, F., Revilla-Romero, B., Salamon, P., De Groeve, T., & Hirpa, F. (2015). The benefit of continental flood early warning systems to reduce the impact of flood disasters.
- Trenberth, K. E., Dai, A., Rasmussen, R. M., & Parsons, D. B. (2003). The changing character of precipitation. *Bulletin of the American Meteorological Society*, *84*(9), 1205–1218. <https://doi.org/10.1175/BAMS-84-9-1205>
- Trigg, M. A., Birch, C. E., Neal, J. C., Bates, P. D., Smith, A., Sampson, C. C., et al. (2016). The credibility challenge for global fluvial flood risk analysis. *Environmental Research Letters*, *11*(9), 094014. <https://doi.org/10.1088/1748-9326/11/9/094014>
- Tulbure, M. G., Broich, M., Stehman, S. V., & Kommareddy, A. (2016). Surface water extent dynamics from three decades of seasonally continuous Landsat time series at subcontinental scale in a semi-arid region. *Remote Sensing of Environment*, *178*(Supplement C), 142–157. <https://doi.org/10.1016/j.rse.2016.02.034>
- Vaze, J., Post, D. A., Chiew, F. H. S., Perraud, J. M., Viney, N. R., & Teng, J. (2010). Climate non-stationarity—Validity of calibrated rainfall-runoff models for use in climate change studies. *Journal of Hydrology*, *394*(3-4), 447–457. <https://doi.org/10.1016/j.jhydrol.2010.09.018>
- Vorogushyn, S., Bates, P. D., Bruijn, K. d., Castellarin, A., Kreibich, H., Priest, S., et al. (2018). Evolutionary leap in large-scale flood risk assessment needed. *Wiley Interdisciplinary Reviews: Water*, *5*(2), e1266. <https://doi.org/10.1002/wat2.1266>
- Wahlstrom, M., & Guha-Sapir, D. (2015). *The human cost of weather related disasters*. Geneva, Switzerland: UNISDR.
- Ward, P. J., Jongman, B., Salamon, P., Simpson, A., Bates, P., De Groeve, T., et al. (2015). Usefulness and limitations of global flood risk models. *Nature Climate Change*, *5*(8), 712–715. <https://doi.org/10.1038/nclimate2742>
- Wetterhall, F., Pappenberger, F., Alfieri, L., Cloke, H., Thielen-del Pozo, J., Balabanova, S., et al. (2013). HESS opinions “Forecaster priorities for improving probabilistic flood forecasts”. *Hydrology and Earth System Sciences*, *17*(11), 4389–4399. <https://doi.org/10.5194/hess-17-4389-2013>
- Wu, H., Adler, R. F., Tian, Y., Huffman, G. J., Li, H., & Wang, J. (2014). Real-time global flood estimation using satellite-based precipitation and a coupled land surface and routing model. *Water Resources Research*, *50*, 2693–2717. <https://doi.org/10.1002/2013WR014710>
- Xu, T., Han, W., Hutchinson, M., Pauwels, J., Whitley, R., & Evans, B. (2018). Potential evapotranspiration: eMAST-R-Package 2.0, 0.01 degree, Australian Coverage, 1970-2012. Retrieved from: <http://geonetworkr9.nci.org.au/geonetwork/srv/eng/catalog.search#/metadata/98afdcd04-d30a-4dfc-a264-4de552482fde>, <http://portal.tern.org.au/potential-evapotranspiration-emast-1970-2012>
- Yamazaki, D., de Almeida, G. A. M., & Bates, P. D. (2013). Improving computational efficiency in global river models by implementing the local inertial flow equation and a vector-based river network map. *Water Resources Research*, *49*, 7221–7235. <https://doi.org/10.1002/wrcr.20552>
- Yamazaki, D., Ikeshima, D., Tawatari, R., Yamaguchi, T., O'Loughlin, F., Neal, J. C., et al. (2017). A high-accuracy map of global terrain elevations. *Geophysical Research Letters*, *44*, 5844–5853. <https://doi.org/10.1002/2017GL072874>
- Yamazaki, D., Kanae, S., Kim, H., & Oki, T. (2011). A physically based description of floodplain inundation dynamics in a global river routing model. *Water Resources Research*, *47*, W04501. <https://doi.org/10.1029/2010WR009726>

- Zhao, F., Veldkamp, T., E. I., Frieler, K., Schewe, J., Ostberg, S., et al. (2017). The critical role of the routing scheme in simulating peak river discharge in global hydrological models. *Environmental Research Letters*, *12*(7), 075003. <https://doi.org/10.1088/1748-9326/aa7250>
- Zhu, Z., Oberg, N., Morales, V. M., Quijano, J. C., Landry, B. J., & Garcia, M. H. (2016). Integrated urban hydrologic and hydraulic modelling in Chicago, Illinois. *Environmental Modelling & Software*, *77*, 63–70. <https://doi.org/10.1016/j.envsoft.2015.11.014>
- Zischg, A. P., Felder, G., Weingartner, R., Quinn, N., Coxon, G., Neal, J., et al. (2018). Effects of variability in probable maximum precipitation patterns on flood losses. *Hydrology and Earth System Sciences*, *22*(5), 2759–2773. <https://doi.org/10.5194/hess-22-2759-2018>